The Polar Cap (PC) index: invalid index series and a different approach.

Peter Stauning[1,1]

[1]Danish Meteorological Institute

November 30, 2022

Abstract

The Polar Cap (PC) indices are derived from the magnetic variations generated by the transpolar convection of magnetospheric plasma and embedded magnetic fields driven by the interaction with the solar wind. The PC indices are potentially very useful for Space Weather monitoring and forecasts and for related research. However, the PC index series in the near-real time and final versions endorsed by the International Association for Geomagnetism and Aeronomy (IAGA) are considered unreliable. Both versions include solar wind sector (SWS) effects in the calculation of the reference levels from which magnetic disturbances are measured. The SWS effects are caused by current systems in the dayside Cusp region related to the Y-component, B, of the Interplanetary Magnetic Field (IMF). However, the IAGA-endorsed handling of SWS effects may generate unfounded PC index changes of up to 3 mV/m at the nightside away from the Cusp. For the real-time PCN and PCS indices, the cubic spline-based reference level construction may cause additional unjustified index excursions of more than 3 mV/m with respect to the corresponding final index values. Noting that PC index values above 2 mV/m indicate geomagnetic storm conditions, such unjustified contributions are considered to invalidate the IAGA-endorsed PC index series. Alternative derivation methods are shown to provide more consistent index reference levels for both final and real-time PC indices, to reduce their unfounded excursions, and to significantly increase their reliability.

1

2

3

4   **The Polar Cap (PC) index: invalid index series and a different approach.**

5

6   Peter Stauning

7   Danish Meteorological Institute, Copenhagen, Denmark

8   Mail: pst@dmi.dk

9

10   **Abstract.**

11   The Polar Cap (PC) indices are derived from the magnetic variations generated by the transpolar
12   convection of magnetospheric plasma and embedded magnetic fields driven by the interaction with
13   the solar wind. The PC indices are potentially very useful for Space Weather monitoring and
14   forecasts and for related research. However, the PC index series in the near-real time and final
15   versions endorsed by the International Association for Geomagnetism and Aeronomy (IAGA) are
16   considered unreliable. Both versions include solar wind sector (SWS) effects in the calculation of
17   the reference levels from which magnetic disturbances are measured. The SWS effects are caused
18   by current systems in the dayside Cusp region related to the Y-component, B_Y, of the Interplanetary
19   Magnetic Field (IMF). However, the IAGA-endorsed handling of SWS effects may generate
20   unfounded PC index changes of up to 3-4 mV/m at the nightside away from the Cusp. For the real-
21   time PCN and PCS indices, the cubic spline-based reference level construction may cause
22   additional unjustified index excursions of more than 3 mV/m with respect to the corresponding final
23   index values. Noting that PC index values above 2 mV/m indicate geomagnetic storm conditions,
24   such unjustified contributions are considered to invalidate the IAGA-endorsed PC index series.
25   Alternative derivation methods are shown to provide more consistent index reference levels for both
26   final and real-time PC indices, to reduce their unfounded excursions, and to significantly increase
27   their reliability.

28

1. Introduction.

The Polar Cap (PC) indices, PCN (North) and PCS (South) are based on magnetic data recorded at the central polar cap observatories in Qaanaaq (Thule) in Greenland and Vostok in Antarctica, respectively. The PC index concept was developed through the pioneering works of Troshichev and Andrezen (1985) and Troshichev et al. (1988). Further PC index developments were made by Vennerstrøm (1991). A fundamental description of the PC index derivation methods and their physical meaning was published by Troshichev et al. (2006).

To derive PC index values, magnetic variations related to the transpolar convection of plasma and magnetic fields are calibrated to equal values of the merging electric field (Kan and Lee, 1979) in the undisturbed solar wind. Thus, the PC indices represent the merging processes between the solar wind magnetic fields extending from the Sun and the terrestrial magnetic fields at the front of the magnetosphere and could be considered representative of the energy input from the solar wind. This energy may be temporarily stored in the magnetospheric tail configuration to be dissipated in processes such as auroral substorms, upper atmosphere heating, and ring current enhancements.

Final (post-event) PCN and PCS index series have been used to investigate relations between interplanetary parameters and polar cap magnetic disturbances (e.g., Troshichev and Lukianova, 2002; Huang, 2005) and the electric potentials in the polar cap ionosphere (e.g., Troshichev et al., 2000; Nagatsuma, 2002; Ridley and Kihn, 2004).

The relations between the polar cap indices and auroral activity was studied, among others, by Troshichev and Andrezen (1985), Vennerstrøm et al. (1991), Vassiliadis et al. (1996), Liou et al. (2003), and Huang (2005). The relations between positive and negative PC index values and Joule heating of the atmosphere was investigated by Chun et al. (1999, 2002). Most investigations have given correlation coefficients ranging between 0.6 and 0.8 between polar cap index values and parameters characterizing auroral activity.

In substorm studies, Janzhura et al. (2007) have used the PC indices to predict the duration of the growth phase in substorm developments. For isolated events they estimated that substorm onset would occur as the PC index level reached ~2 mV/m From investigations of a large number of substorms, Troshichev et al. (2014) concluded that substorm onset was likely to happen when the PC index starting from a low level exceeded 1.5 ±0.5 mV/m.

In studies of geomagnetic storms by Stauning et al. (2008) and Stauning (2012), the PC indices have been used in source functions to predict the development of ring current intensities characterized by Dst index values. Troshichev and Sormakov (2017) have used PC indices to predict the maximum geomagnetic storm intensities (Dst minima).

An important application of real-time PC indices is the forecast of strong substorms that may threaten power grids through their Geomagnetically Induced Current (GIC) effects. An investigation of GIC-related high voltage power line disturbances in Scandinavia (Stauning, 2013c) has demonstrated that the PC index values most often remained at a high level for more than 2-3 hours up to the power line cuts. The lengthy pre-event intervals are most likely needed for enabling the merging processes at the front of the magnetosphere and subsequent transpolar convection characterized by the PC index to load the tail configuration with enough energy to generate violent substorm events. The intense merging processes may also be necessary for making the polar cap expand enough to enable substorm activity reaching subauroral latitudes where important power grids reside. According to these investigations, PC index levels above 10 mV/m maintained through more than one hour should cause alert for subauroral power grids (Stauning, 2020).

In the past, a diversity of PC index versions have been in play at the above-mentioned (and many further) investigations (Stauning, 2013a), which seriously reduce their scientific value. Thus, much

75 effort has been invested in attempts to generate commonly accepted PC index versions (e.g.,
76 Troshichev et al., 2006; Stauning et al., 2006). On basis of the documentation provided in Matzka
77 (2014), new PC index versions were adopted by IAGA by its Resolution no. 3 (2013) with the text:

78 *IAGA, **noting** that polar cap magnetic activity is not yet described by existing IAGA geomagnetic*
79 *indices, **considering** that the Polar Cap (PC) index constitutes a quantitative estimate of*
80 *geomagnetic activity at polar latitudes and serves as a proxy for energy that enters into the*
81 *magnetosphere during solar wind-magnetosphere coupling, **emphasising** that the usefulness of such*
82 *an index is dependent on having a continuous data series, **recognising** that the PC index is derived*
83 *in partnership between the Arctic and Antarctic Research Institute (AARI, Russian Federation) and*
84 *the National Space Institute, Technical University of Denmark (DTU, Denmark) **recommends** use*
85 *of the PC index by the international scientific community in its near-real time and definitive forms,*
86 *and **urges** that all possible efforts be made to maintain continuous operation of all geomagnetic*
87 *observatories contributing to the PC index.*

88 Thus, the IAGA-recommendations comprise both the final and the near-real time versions of PCN
89 and PCS indices. Until the final values could be issued, the indices may be available in provisional
90 versions. At present, the PCN indices are distributed in all versions, while the PCS indices are
91 distributed in their near-real time and provisional versions only. The indices are distributed from the
92 web portals http://pcindex.org operated by AARI and http://isgi.unistra.fr operated by the
93 International Service for Geomagnetic Indices (ISGI). However, as shall be demonstrated, the near-
94 real time values as well as the final PC index series are invalidated by inappropriate handling of the
95 solar wind sector effects in reference level calculations.

96

97 **2. Calculation of Polar Cap indices.**

98 The transpolar (noon to midnight) convection of plasma and magnetic fields driven by the
99 interaction of the solar wind with the magnetosphere generates electric (Hall) currents in the upper
100 atmosphere. These currents, in turn, induce magnetic variations at ground level (Troshichev et al.,
101 1988, 2006; Vennerstrøm, 1991). For derivation of PC indices from the recorded magnetic field
102 series, $\mathbf{F}$, the horizontal magnetic variations, $\Delta\mathbf{F} = \mathbf{F} - \mathbf{F}_{RL}$, with respect to an undisturbed reference
103 level (RL), $\mathbf{F}_{RL}$, are projected to a direction in space assumed to be perpendicular to the transpolar
104 convection-related currents in order to focus on solar wind effects. The optimum direction is
105 characterized by its angle, φ, to the E-W direction. Next, ΔF_{PROJ} values are scaled to make the PC
106 index equal on the average to the solar wind merging electric field, E_M, (Kan and Lee, 1979). Thus

107 $\quad PC = (\Delta F_{PROJ} - \beta)/\alpha \approx E_M$ (1)

108 The optimum angle, φ, and the propagation delay, τ, between the reference location for the solar
109 wind data and the location for related effects at the polar cap are both estimated from searching the
110 optimum correlation between E_M and ΔF_{PROJ}. The calibration constants, the slope, α, and the
111 intercept, β, are found by linear regression between ΔF_{PROJ} and E_M through an extended epoch of
112 past data.

113

114 **3. PC index reference level.**

115 For the reference level from which polar magnetic disturbances are measured, different concepts
116 have been used. In the version developed by Vennerstrøm (1991), just the secularly varying base
117 level, $\mathbf{F}_{BL}$, was used. This level does not reflect the daily magnetic variations during undisturbed
118 conditions. However, the calibration parameters, notably the intercept coefficient, reflect the
119 undisturbed daily variation averaged over the epoch used for the regression.

120    $\mathbf{F}_{RL} = \mathbf{F}_{BL}$ (Vennerstrøm, 1991)   (2)

121 In the version developed at the Arctic and Antarctic Research Institute (AARI) in St. Petersburg,
122 Russia, the varying level on "*extremely quiescent days*" (Troshichev et al., 2006) was used as the
123 PC index reference level. This level could be considered built from a quiet day curve (QDC), $\mathbf{F}_{QDC}$,
124 added on top of the base level, $\mathbf{F}_{BL}$. Thus in vector formulation:

125    $\mathbf{F}_{RL} = \mathbf{F}_{BL} + \mathbf{F}_{QDC}$ (AARI, Troshichev et al., 2006)   (3)

126 Extremely quiescent days are rare particularly at polar latitudes. Therefore, the concept was
127 broadened to imply the generation of QDC values from quiet segments of nearby days. The QDC
128 calculations are detailed in Janzhura and Troshichev (2008) (hereinafter J&T2008). From the
129 recordings during 30 days at a time, the variability in the 1-min samples within each 20-min section
130 of recorded data is used to decide whether the section is quiet enough to let the average value be
131 included in the construction of an initial QDC by superposition of quiet samples. The particular day
132 for the QDC is determined by the relative amounts of quiet samples and usually positioned at the
133 middle of the considered interval. The 30 days interval is then shifted forward and the QDC
134 calculations repeated to be referred to another (or eventually the same) day. Finally, from the
135 sequence of initial 30-days QDCs the final QDCs for any of the days are found by smoothing
136 interpolation. It should be noted that the choice of using 30 days interval at a time implies evening
137 out possible solar wind sector (SWS)-related effects which may have cyclic variations with the 27.4
138 days solar rotation. (the notation "SWS" is used here instead of "SS" used elsewhere).

139 In order to handle the SWS-related variations, $\mathbf{F}_{SWS}$, caused mainly by the effects from the Y-
140 component, IMF B_Y, of the Interplanetary Magnetic field (IMF), on the convection patterns, it was
141 suggested by Menvielle et al. (2011) that the reference level should be constructed from using a
142 particular solar wind sector term, $\mathbf{F}_{SWS}$, added to the base level and the regular QDC.

143    $\mathbf{F}_{RL} = \mathbf{F}_{BL} + \mathbf{F}_{QDC} + \mathbf{F}_{SWS}$ (Menvielle et al., 2011)   (4)

144 It should be noted that this concept marks an infringement of the QDC definition in Troshichev et
145 al. (2006) by introducing a reference level contribution, $\mathbf{F}_{SWS}$, which is not necessarily quiet. There
146 is no validation of this concept or reference to its origin in Menvielle et al. (2011).

147 The SWS concept is further specified in Janzhura and Troshichev (2011) (hereinafter J&T2011). At
148 the interaction between the solar wind and the magnetosphere, as explained in J&T2011, the IMF
149 B_Y components generate field-aligned currents (FAC) and associated horizontal currents in the
150 Cusp region near local noon at 75-80° geomagnetic latitude. In p. 1492 of J&T2011 they state that
151 "*the QDC level displays long-term changes, which are determined by the sector structure*". Further
152 they state "*Thus, if we are going to analyze the polar cap magnetic activity produced by the IMF*
153 *fluctuations related to disturbed solar wind, we have to exclude first the sector structure effect*".

154 One implication of their statement is that the IMF B_Y component when varying slowly (few days to
155 2 weeks) is not affecting the polar magnetic disturbance levels. The issue has not been properly
156 validated and the implication might be incorrect. The second issue, which shall be discussed to
157 some extent here, is whether the applied data handling techniques actually remove the sector
158 structure effects or just (as will be shown) generate inconsistent features and odd results.

159 In J&T2011 the sector structure effects are derived from daily median values of the recorded polar
160 magnetic fields that vary with the IMF B_Y component in the solar wind. In the post-event version,
161 the SWS terms are derived from daily median values smoothed over 7 days with the day of interest
162 at the middle. In the near-real time version the actual day's SWS value is derived by cubic spline-
163 based extrapolation of past daily median values. The regular 30-days QDC is derived from the
164 recorded data less the SWS effect. Thus:

165        $\mathbf{F}_{RL} = \mathbf{F}_{BL} + \mathbf{F}_{SWS} + \mathbf{F}_{QDC,SWS}$ (Janzhura and Troshichev, 2011)   (5)

166 For the IAGA-endorsed version (Matzka, 2014), the base level in the AARI version in Eq. 3
167 (Troshichev et al., 2006) is replaced by a median-based level, $\mathbf{F}_M$. The modified QDC term,
168 $\mathbf{F}_{QDC,SWS}$, is derived from the data series, $\mathbf{F}$, less the $\mathbf{F}_M$ values.

169        $\mathbf{F}_{RL} = \mathbf{F}_M + \mathbf{F}_{QDC,SWS} = \mathbf{F}_{BL} + \mathbf{F}_{SWS} + \mathbf{F}_{QDC,SWS}$ (IAGA, Matzka, 2014)   (6)

170 Actually, this is the same concept as the one defined in J&T2011 except that the secular variations
171 are now included in the median values (Nielsen and Willer, 2019) instead of being included in the
172 base line values. Thus, the IAGA concept could be discussed on basis of the J&T2011 publication,
173 which – so far – holds the only existing presentation of the QDC and SWS properties issued from
174 the providers of the IAGA endorsed PC indices. The SWS concept has been discussed in Stauning
175 (2013b, 2015, and 2018a,c).

176

177 **4. Reference levels for PC index calculations in the IAGA-endorsed post-event (final) version.**

178 The IMF B_Y-related variations in the daily course of the polar magnetic field components are
179 important for calculations of the reference level for PC index calculations. It should be noted that
180 the local time 24 h cycle represents the daily course in the observatory position relative to the Cusp
181 region located close to local noon at magnetic latitudes a few degrees equatorward of Qaanaaq
182 latitude.

183 Like noted at p. 1492 in J&T2011, "*the azimuthal IMF component controls the BY FAC* (field-
184 aligned current) *system observed in the day-time cusp region during the summer season*". Thus, the
185 anticipated IMF B_Y-related effects on the convection patterns should maximize near noon and be
186 reduced near midnight when the observatory location is farthest away from the Cusp. For Qaanaaq
187 data this tendency is seen most clearly in displays of the H- (or Y-) component variations.

188 The interval from days 145 to 245 of 2001 is discussed in J&T2011 and therefore selected for a
189 closer examination of data and derived values here. Fig. 5b of J&T2011 displays the average daily
190 variations in the H-components (all samples) recorded at Qaanaaq during the summer months, May-
191 August, of 2001 for different levels of IMF By. For the same data interval, Fig. 1 here displays the
192 corresponding IMF B_Y-related daily variations for the quietest days only. Values of the IMF B_Y
193 component   are   derived   from   OMNIweb   interplanetary   satellite   data   service
194 (http://omniweb.gsfc.nasa.gov).

195 The results in Fig. 1 are largely the same as those of Fig. 5b in J&T2011. Local midnight at
196 Qaanaaq is at around 04 UT, noon at 16 UT. It is seen in both diagrams that the variations with IMF
197 B_Y are small during the night while the daytime values, and thus the amplitude in the daily
198 variations, depend strongly on the IMF By level.

199
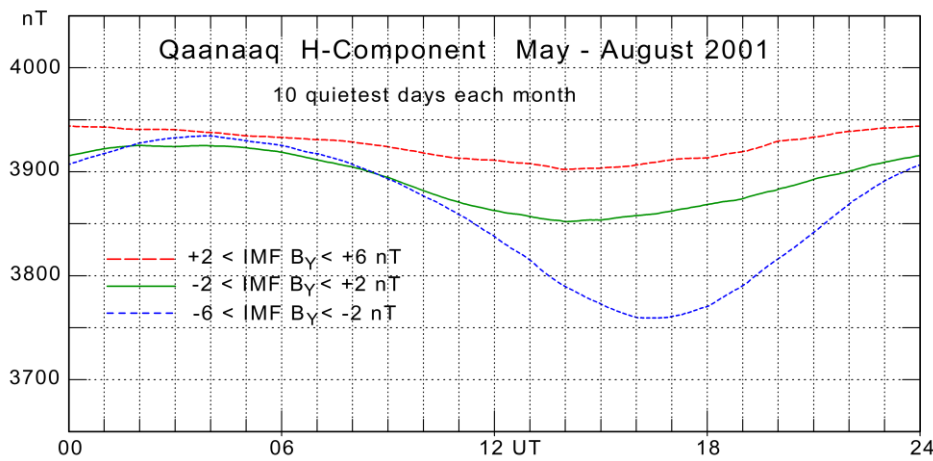
Figure 1. Mean daily variation in the H-component at Qaanaaq (Thule) during the 10 quietest days of each
of the summer months of 2001 derived for three gradations of the IMF azimuthal component: $+2 < B_Y <+6$
nT (upper red line), $-2< B_Y <2$ nT (green line), and $-6 < By <-2$ nT (lower blue line).

With the variations of the QDC values with IMF B_Y displayed in Fig. 1 during the months centered
on 1 July and corresponding displays centered at different dates, the QDC values throughout the
selected interval could be constructed. The resulting QDCs taking the seasonal as well as the IMF
B_Y-related variations into account are displayed by the curve in heavy red line superimposed on the
observed values of the H-component shown in Fig. 2. Smoothed values of IMF B_Y are displayed by
the lover curve with reference to the right scale. The upper envelope of the QDC values presents the
night H-component values and varies little with IMF B_Y while the lower envelope, which presents
the midday QDC values, varies strongly with IMF B_Y in agreement with the display in Fig. 1. These
QDCs could be considered to represent idealized QDC levels for the summer season of year 2001.
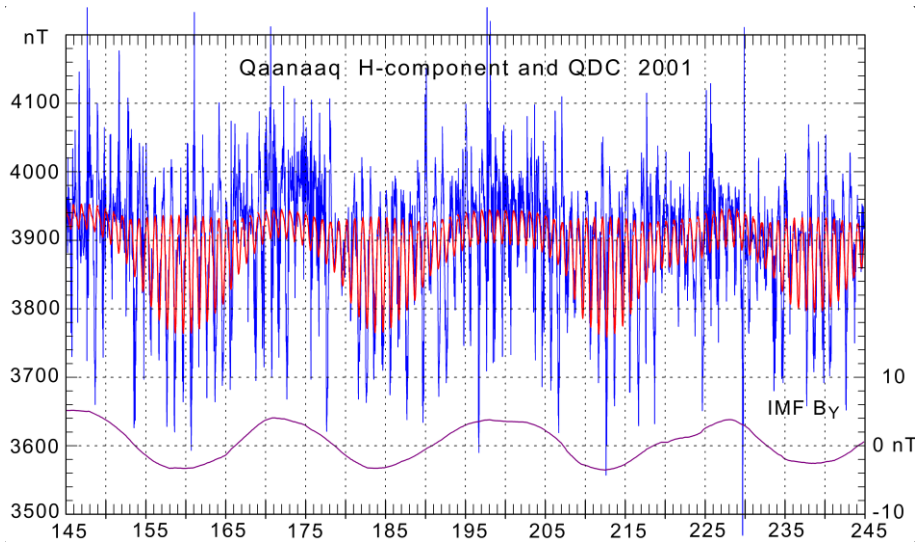
Figure 2. QDCs (red line) based on quiet data only superimposed on recorded H-component values (blue
line). Smoothed values of IMF B_Y (magenta line) on right scale are shown at the bottom.

For the IAGA-endorsed post-event (final) PC index version, Fig. 3 displays the construction of the
reference levels. The upper three fields are based on interim values derived from PCN index
calculations and supplied from the PCN index provider at DTU Space. For reference, the bottom
curve (f) displays smoothed values of the IMF B_Y component (same as those displayed in Fig. 2).
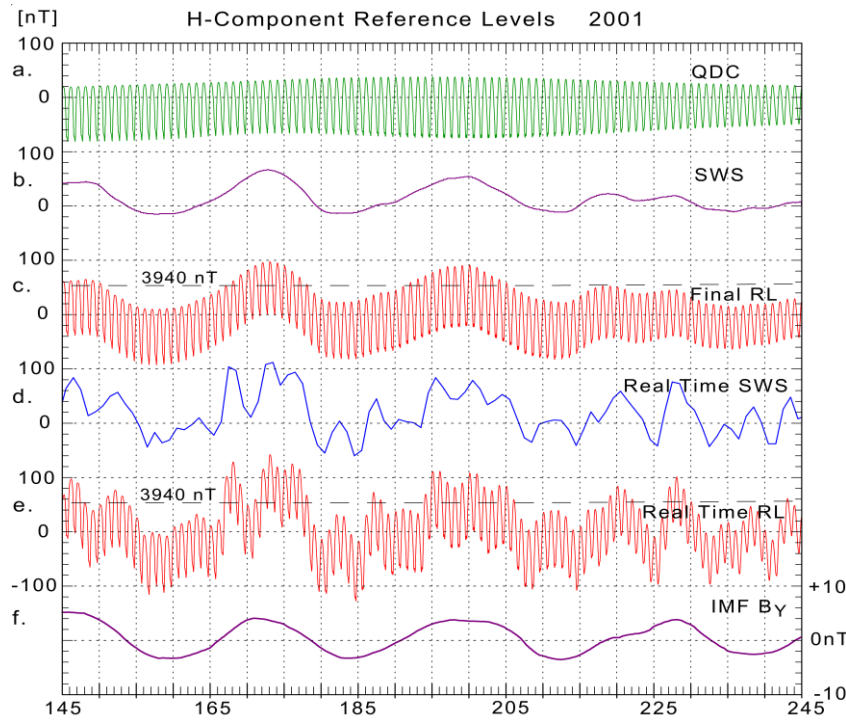
Figure 3. IAGA-endorsed constructions of H-component reference levels for PCN throughout days 145 to 245 of 2001 for final and real-time PCN index versions. (a.) Final QDC_{SWS}. (b.) Final SWS terms. (c.) Final reference levels, RL. (d.) Real-time SWS terms. (e.) Real-time reference levels. (f.) Smoothed IMF B_Y (on right scale).

The upper curve (a) in Fig. 3 displays the 30-days QDC_{SWS} values for the Qaanaaq H-component derived according to the method defined in J&T2008 but based on recorded quiet data less the SWS terms. The next lower curve (b) displays the SWS terms derived as the differences (cf. Eq. 6) between the 7-days smoothed daily median values and the secularly varying base line values interpolated between the yearly defined values (also supplied from DTU Space). The 0 nT dotted line represents base line values varying between 3895 nT on day 145 and 3899 nT on day 245.

The next lower curve (c) displays the resulting H-component reference level formed as the sum of the H_{SWS} and $H_{QDC,SWS}$ values (cf. Eq. 5). The horizontal dashed line across this curve (c) presents the uppermost level (3940 nT) of the mean H-component values in Fig. 1 (or Fig. 5 of J&T12011). Curve (c) is an almost exact replica of the H-component reference curve displayed in heavy line in Fig. 1 of J&T2011 for which the caption states "*the quiet daily curve (QDC) characterizing the daily variation of the quiet geomagnetic field*". However, there are serious problems with this choice of reference level:

(i) Contrary to the caption for Fig. 1 of J&T2011, the reference level is not "quiet" being composed from the sum of a quiet part and a median-based part that varies with the disturbance level.

(ii) The daily variations in the components imposed by the reference level construction are not in agreement with observed daily variations during corresponding conditions.

(iii) The upper envelope which represents night values of the daily variations in the H-component varies strongly with the varying IMF B_Y level contrary to night values in Fig. 1 (or Fig. 5 of J&T2011). Some of the night reference values exceed considerably the uppermost statistical average values for corresponding IMF B_Y conditions whether based on all data (Fig. 5 of J&T2011) or just quiet values (Fig. 1 here).

252 (iv) The amplitudes in the daily variation display seasonal variations only and do not vary with the
253 IMF B_Y level contrary to the strong amplitude variations seen in Fig. 1 (or Fig. 5 of J&T2011). For
254 June (days 152-181) of 2001 the amplitudes in the reference level variations remain at appr. 100 nT,
255 while in Fig. 1 the amplitudes vary with the relevant IMF B_Y levels (-3 to +4 nT) between appr. 50
256 and 150 nT.

257 (v) Using the reference levels from Fig. 3 and the corresponding levels for the D-component at
258 index calculations generates peculiar daily variations in the SWS-related contributions to the PCN
259 index.

260 The SWS term, $\mathbf{F}_{SWS}$, is a vector rotating with the Earth and must be projected to the optimum
261 direction in space to derive its contribution to the PC index. During 24 hours the projected term
262 varies between + and – the maximum amplitude reached at two locations, one at daytime the other
263 at night, when the $\mathbf{F}_{SWS}$ direction is parallel (or antiparallel) to the optimum direction. According to
264 Eq. 1, the effect on the PC index is $\Delta PC_{SWS} = F_{SWS,PROJ} / \alpha$. The slope values, α, are around two
265 times larger at day than at night (cf. coefficient tables at http://pcindex.org). Thus, with the present
266 calculation scheme, the nighttime ΔPC_{SWS}, inevitably, will be around twice the daytime
267 contributions although the IMF B_Y-related SWS effects caused by current systems at the Cusp
268 region near noon in local time (Wilhjelm et al., 1972; Iijima and Potemra, 1976) should maximize
269 there and be minimal at night. This obvious conflict was addressed in Stauning (2013b and 2015).

270 Using both the H- and the D-components (or the X- and Y-components) of the data supplied from
271 DTU Space enables specific calculations of the SWS effects on the PCN indices. The calibration
272 parameters (φ,α,β) published at http://pcindex.org by the index providers have been used in the
273 calculation of the contributions. The result for a selected day, 22 June 2001, is shown in Fig. 4.
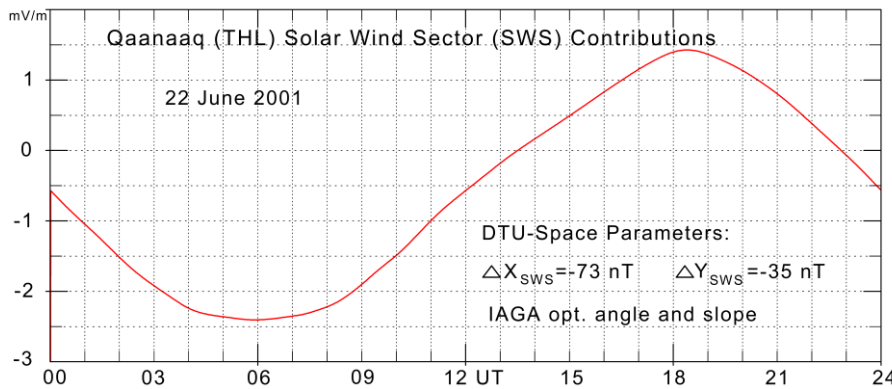
275 **Figure 4**. Variations in the SWS-related contributions to the PCN index on 22 June 2001 based on data and
276 base line values supplied from DTU Space. (similar to Fig. 4 of Stauning, 2015)
277

278 The display in Fig. 4 based on the data supplied from DTU Space is very close to the results
279 presented in Fig. 4 of Stauning (2015) based on the data presented in J&T2011. The most
280 controversial feature is the (numerical) maximum in the IMF B_Y-related SWS contributions to the
281 PCN index values at night with a depression of 2.5 mV/m at 06:30 UT near local midnight (04 UT).
282 At this time, the THL observatory is farthest away from the Cusp region where the IMF B_Y-related
283 effects originate. The contribution is small at local noon (16 UT) where the observatory is closest to
284 the Cusp region. The largest positive contribution of 1.5 mV/m is seen at 18:30 UT, a few hours
285 past local noon.

286 A basic error in the method is the implied assumption that a SWS term calculated from daily
287 median values can be applied throughout the whole day to remove SWS effects disregarding the
288 variations of the IMF B_Y–related solar wind sector effects with the varying observatory position in

289 the polar cap. The real SWS effects could even be opposite of the effects calculated from the
290 constructed SWS values derived by the median-based method.

291 The example calculations displayed in Fig. 4 were based on the case presented in J&T2011 with a
292 smoothed IMF B_Y value of 4 nT, which is not uncommon. Unjustified SWS contributions of 3-4
293 mV/m could be expected for the stronger cases (larger IMF B_Y). Such magnitudes are around twice
294 the onset level of around 2 mV/m for magnetic storm or substorm activity (Troshichev et al., 2014).

295

296 **5. Reference levels for PC index calculations in the IAGA-endorsed near-real time version.**

297 For real-time calculations of PC index values, which is an important issue for Space Weather
298 monitoring and forecasting, the 7-day smoothing of median values used for the final version is no
299 longer applicable. Instead, a cubic spline extrapolation method specified in J&T2011 is applied to
300 derive the actual SWS terms from past median values. The method uses 3-days average median
301 values calculated every other of the past 9 days to derive cubic spline polynomials, which are
302 subsequently extended forward to define the actual SWS value. Based on data from the examined
303 interval of June 2001, the method is illustrated in Fig. 5 using the terminology from J&T2011.

304
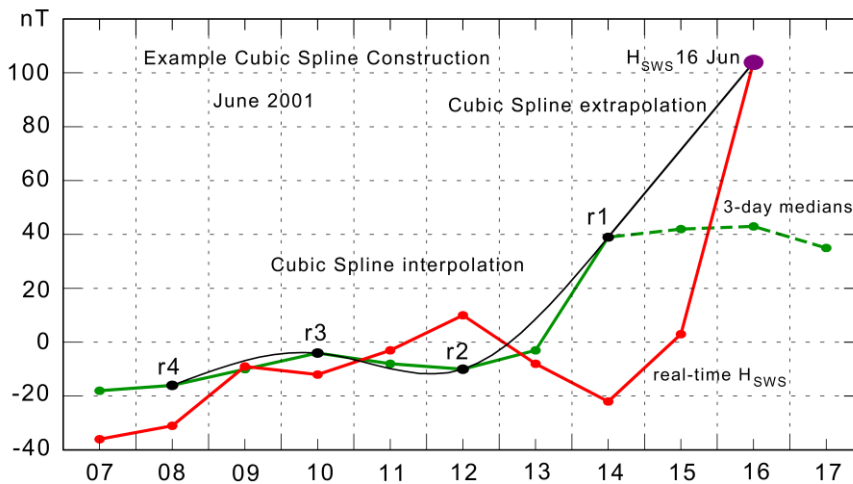
Figure 5. Details of the cubic spline construction (in black line) of the real-time solar sector term, H_{SWS},
from 3-day medians (in green line). The selected four 3-day median values used for the construction of H_{SWS}
on 16 June 2001 are marked by black dots superimposed on the green ones. The cubic spline interpolation
curve and its extrapolation to define real-time H_{SWS} on 16 June are displayed in black line. The dots
connected by the red line represent H_{SWS} values derived by the same method on earlier dates in June 2001.

311 Fig. 5 demonstrates the cubic spline construction for deriving the SWS term on 16 June, 2001. The
312 3-day median values (green dots) named according to the J&T2011 procedure by r1 (13-15), r2 (11-
313 13), r3 (9-11), and r4 (7-9 June) are marked by black dots superimposed on the green ones. The
314 natural cubic spline polynomials have been derived from these 4 points and define the curve in
315 black line connecting the points. With the slope defined at the last point (14 June) the cubic spline
316 construction is extended tangentially to 16 June where the resulting H_{SWS} value (103 nT) is marked
317 by a large black dot.

318 The dots (red) connected by a red line display the H_{SWS} values derived the same way for further
319 days within the interval from 7 to 16 June using past data only. The 3-day median values on 15, 16
320 and 17 June connected by the green dashed line segments were not available at the real-time
321 construction of H_{SWS} for 16 June. They have been added to the figure for illustration of the "take-
322 off" effects of the cubic spline extrapolation construction that generates the large deviation of the

323 extrapolated SWS values compared to the post-event smoothed values (cf. Figs. 3 and 6). This is an
324 inherent effect when using the devised "near-real time" method from J&T2011 to calculate solar
325 sector effects. A similar figure for a different interval may be seen in Stauning, 2018c.

326 The real time H_{SWS} values for 7-16 June 2001 displayed in Fig. 5 along with the corresponding
327 H_{SWS} values calculated the same way for the remainder of the days 145-245 of 2001 have been
328 inserted as the jagged curve (d) in Fig. 3. It should be noted that these values differ from the values
329 presented by the smooth H_{SS} curve in Fig. 6 of J&T2011, which appear, contrary to their statements
330 in p. 1496, to be derived from smoothed median values like the nearly identical values (from DTU
331 Space) displayed by curve (b) in Fig 3. (for the review process, please see an extended examination
332 in appendix A1)

333 According to the principles for near-real time PC index calculations defined in J&T2008, the 30-
334 days QDC should be derived by adjusting the most recent 30-days QDC using the seasonal trend
335 from last year's QDCs. Since the QDCs in the formulation of J&T2011 (or Matzka, 2014) are
336 derived from observed data less the SWS terms there is an obvious flaw in the arguments since the
337 SWS-conditions are not necessarily the same at corresponding dates in different years.

338 Taking a short-cut by assuming that the actual near-real time $H_{QDC,SWS}$ values are the same as the
339 final $H_{QDC,SWS}$ values displayed by curve (a) of Fig. 3 results in the near-real time H-component
340 reference level displayed by curve (e) in Fig. 3. The corresponding process would provide the D-
341 component near-real time values. It is clear from comparing the reference levels defined for the
342 final version (curve c of Fig. 3) with those of the near-real time version (curve e) that PCN values
343 calculated by the near-real time method must differ considerably from index values derived by the
344 post-event method. The resulting effects on the differences between real-time and post-event (final)
345 PCN values throughout June 2001 are displayed in the bottom panel of Fig. 6.

346

347
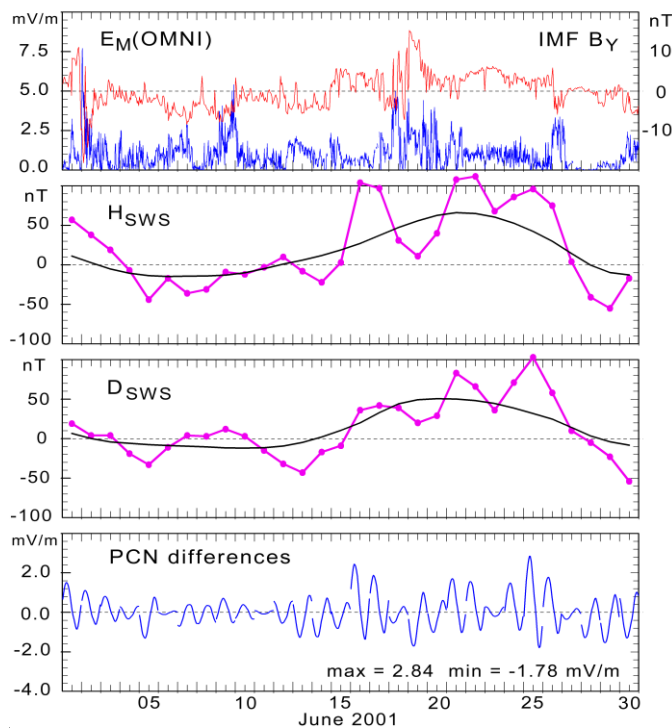
Figure 6. From top: Solar wind merging electric field (blue line, left scale) and IMF B_Y component (red line,
right scale), H_{SWS} (real-time) in magenta line and H_{SWS} (final) in black line, D_{SWS} (real time) and D_{SWS} (final),
and (in bottom panel) differences between real-time and final PCN values. Peak differences are noted.

351

352 The differences of up to 2.84 mV/m have been calculated from the final (smoothed) and the near-
353 real time cubic spline extrapolated SWS vectors using consolidated calibration parameters
354 (http://pcindex.org). The calculated examples agree well with results obtained from occasional
355 downloads of near-real time PCN and PCS values compared to the same index series downloaded at
356 much later times. Differences of up to 3.09 mV/m for PCN (Stauning, 2018c) and up to 3.67 mV/m
357 for PCS (Stauning, 2018a) were found in the examples displayed in Fig. 7. Such differences related
358 to using cubic spline extrapolated instead of smoothed values of SWS terms may come on top of the
359 unjustified SWS contributions discussed in section 4. The examples in Fig. 7, furthermore, indicates
360 that the SWS effects, which generate large index differences by their different handling in the near-
361 real time and post-event versions, are equally strong at the Northern and Southern Polar Caps. This
362 result is contrary to the statement of the opposite in pp. 1492-1493 of J&T2011 where SWS-effects
363 are considered negligible for PCS values derived on basis of magnetic data from Vostok on the
364 Antarctic ice cap.

365
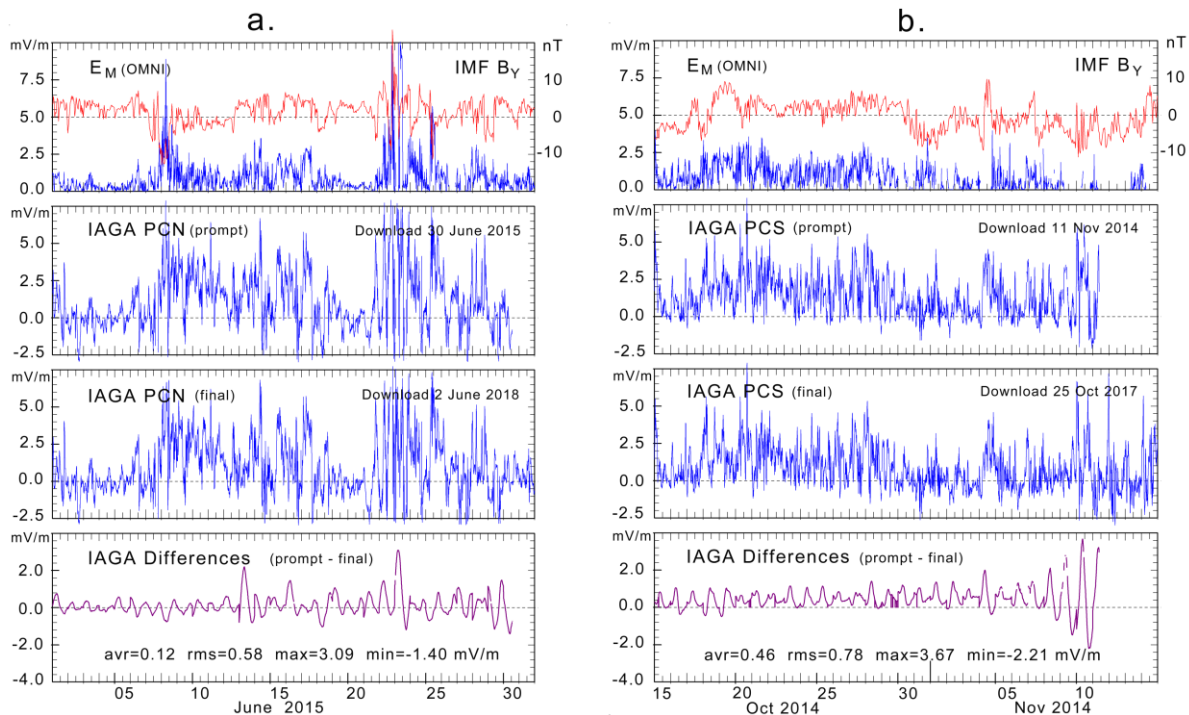
366 **Figure 7**. Differences between IAGA-endorsed versions of recorded 15-min values of near-real
367 time and final PCN (left) and PCS (right) indices. (from Stauning, 2018a,c)
368

369 In Fig. 7 the real-time values are those seen at the end of the traces termed "prompt". The remaining
370 parts of the prompt traces are "post-event" values where the approximation to the "final" values is
371 thought to be gradually improved as more post-event data become available from dates up to the
372 download time. However, the largest excursions, 3.09 mV/m in PCN and -3.67 mV/m in PCS, are
373 seen at dates prior to the real-time days. Details of the IAGA-endorsed calculation methods are not
374 available for further examination of this issue.

375

376 **6. Reference levels for PC index calculations in the DMI version.**

377 In the DMI PC index version (Stauning, 2016), the definition of the "solar rotation weighted"
378 (SRW) reference level construction published in Stauning (2011) returns to the statements in
379 Troshichev et al. (2006) with the vector formulation in Eq. 3, and to the methods outlined in

380 J&T2008. The essential point for the SRW method is deriving the reference level from quiet
381 samples collected at conditions otherwise as close as possible to those prevailing at the day of
382 interest. The factors of primary importance are:

383 (i) Sample "quietness"

384 (ii) Separation of samples from QDC date

385 (iii) Solar wind conditions (particularly IMF B_Y and V_{SW})

386 (iv) Solar UV and X-ray illumination (based on solar radio flux F10.7 values)

387 For these factors weight functions are defined. For each hour of the day, observed hourly average
388 values at corresponding hours within an extended interval (±40 days) are multiplied by the relevant
389 weights, added and then divided by the sum of weights to provide the hourly QDC value.
390 Subsequently, the hourly QDC values are smoothed to remove irregular fluctuations and
391 interpolated to provide any more detailed resolution as required.

392 The weight function for sample quietness is determined from the variability of 1-min data values
393 within the hour much like the technique used by J&T2008. Two parameters are calculated on a
394 vector basis. One is the maximum time derivative used to indicate the smoothness within the sample
395 hour. The other is the average variance to define the slope of data values. Both parameters need to
396 take small values for the hourly sample to be considered "quiet" (flat and featureless display).

397 For an estimate of further weight functions, the factors of importance were subjected to an
398 autocorrelation analysis vs. separation between the date of interest and the dates of the samples to
399 be included in the construction of the QDC values.

400 Details of the autocorrelation are provided in Stauning (2011). The main results were, as expected,
401 high autocorrelation values at nearby dates and also high values at dates displaced one full solar
402 rotation of 27.4 days from the day of interest where the solar illumination and the solar wind
403 conditions were similar on a statistical basis to the prevailing conditions. In between, at half a solar
404 rotation, mixed autocorrelation results were found. In some cases a local maximum was seen
405 indicating the occurrence of 4-sector solar wind structures. In most cases the autocorrelation
406 function had a deep minimum at half a solar rotation indicating 2-sector structures. For the solar
407 rotation weighting a squared cosine function was selected to provide unity weights at the QDC date
408 (zero separation), and at dates separated by 27.4 days, and zero weight at half a solar rotation period
409 when the opposite face of the Sun is pointing toward the Earth and the solar wind sector effect,
410 most likely, is in the opposite direction (2-sector structure) or weak (multi-sector structure) (cf. Fig.
411 6 of Stauning, 2013a).

412 The final weight factors for sample separation have a central maximum holding 50% of the total
413 weights and two secondary maxima at a solar rotation period (27.4 days) before and after the QDC
414 day holding weights corresponding to 25% of the total weight each. The total span of samples
415 included in the QDC construction is set to ±40 days to encompass all three weight maxima. The
416 separation weight factors are pre-calculated (see Stauning, 2011).

417 As data are collected the quietness weight factors can be calculated promptly for each hour of
418 recordings along with the hourly averages of each component. The three values are stored. The
419 quietness weight factors are common for the two horizontal components and independent on their
420 representation in (X,Y) or (H,D) coordinates.

421 Thus, at any time after 80 days of data collection, the relevant final QDC could be calculated for
422 any day more than 40 days in the past. The hourly component averages and their quietness weight
423 factors are fetched from their stored values and their separation weight factors are found from the
424 tabulated values. For each hour of the day, the hourly average component values within ±40 days

425 are multiplied by the weight factors and summarized. The products of weight factors are
426 summarized. The sum of weighted component hourly average values is divided by the sum of
427 weights to define the hourly QDC value.

428 The weighting technique allows calculations of real-time QDCs with reduced accuracy by simply
429 ignoring missing samples without changing the calculation scheme. The DMI SRW-method is
430 illustrated in Fig. 7 in a format similar to Fig. 3 with smoothed values of IMF By displayed by the
431 bottom curve (d). The uppermost curve (a) display H_{QDC} values derived by weighting the samples
432 collected at corresponding hours over ±40 days with their "quietness" factors only disregarding the
433 solar rotation weight factors. Curve (b) displays post-event (final) solar rotation-weighted H-QDC
434 values. The next lower curve (c) displays real-time H-QDC values derived by using the SRW
435 calculation scheme but including pre-event samples only (Half solar rotation weighting, HSRW).
436

437
438
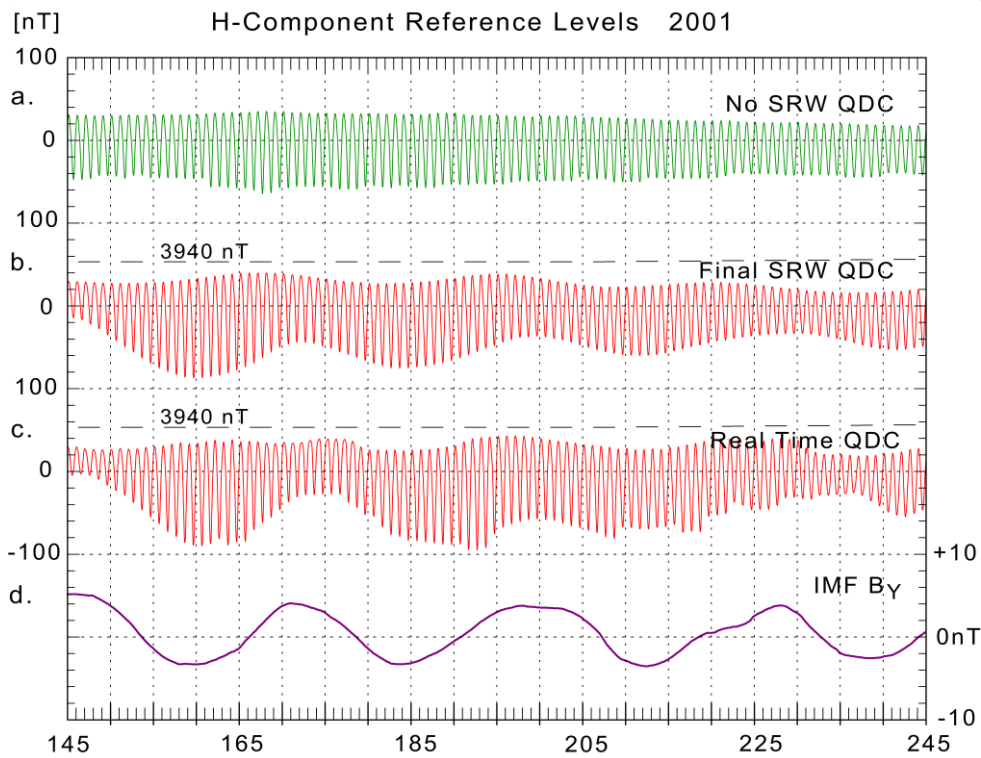
439 **Figure 8.** DMI solar rotation weighted (SRW) QDC reference values. (a) QDC with quietness weighting
440 only. (b) Post-event (final) SRW QDC. (c) Real-time (HSRW) QDC values built from past samples only. (d)
441 Smoothed IMF By values.
442

443 The upper envelope (night values) of the SRW QDC reference values in curve (b) displays small
444 variations with IMF By while the lower envelope (midday values) and the amplitudes in the daily
445 variation display much stronger variations with IMF B_Y as anticipated from the features seen in
446 Figs. 1 and 2 here (and Fig. 5 of J&T2011). The final QDCs in curve (b) should be compared to the
447 reference levels in curve (c) in Fig. 3. The real-time QDCs in curve (c) in Fig. 8 based on using past
448 data only (0 to -40 days) display more irregular variations than the QDCs based on the full amount
449 (±40 days) as could be expected. However, the real-time reference QDCs in curve (c) in Fig. 8
450 should be contrasted to the jagged reference levels displayed by curve (e) in Fig. 3. The horizontal
451 dashed lines across the two middle fields present the uppermost level of average H-component
452 values in Fig. 1 (like those drawn in Fig. 3). It is seen that the QDC reference values here – contrary

453 to the reference levels displayed in Fig. 3 – remain below the uppermost level of statistical mean
454 values for the relevant IMF B_Y ranges.

455 An example of the relations between post-event (final) and real-time PCN index values is depicted
456 in Fig. 9 using data from the previously selected interval spanning days 145-245 of year 2001.

457

458
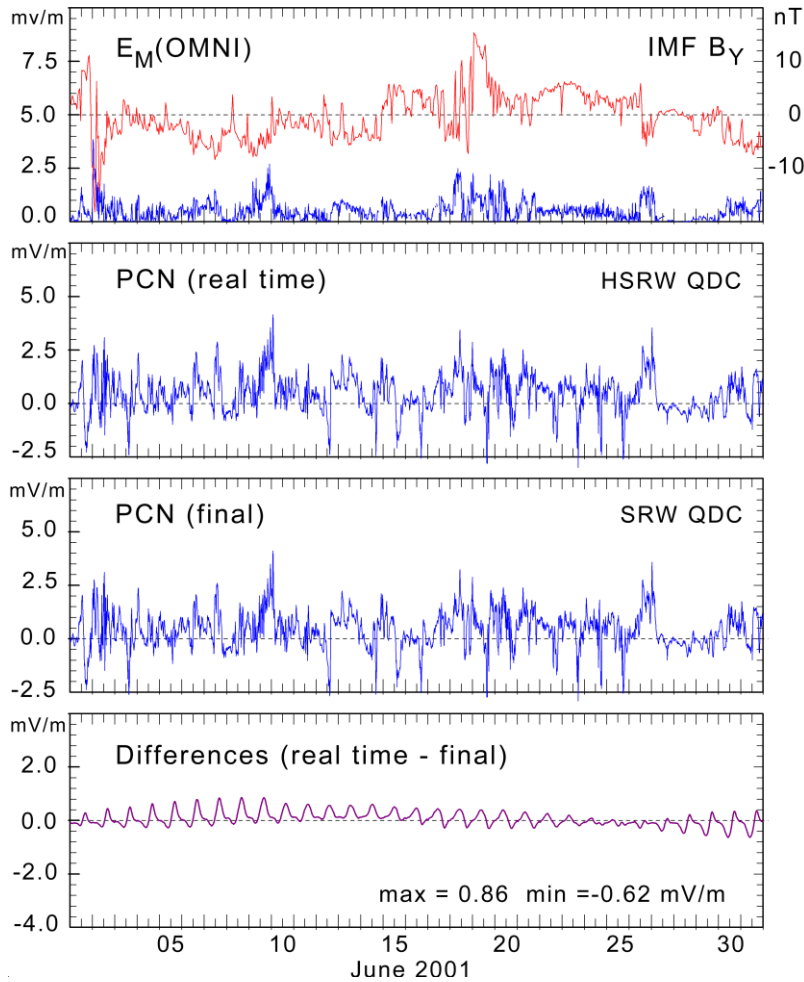
459 **Figure 9**. Example of differences between real-time and final PCN values derived by using HSRW QDCs
460 on past data from days -40 to present day only and SRW QDC using the full ±40 days sampling interval.

461

462 The differences displayed in the bottom field of Fig. 9 should be contrasted to those displayed at the
463 bottom field of Fig. 6 on the same scale. It is seen that the differences between calculated real-time
464 and post-event PCN index values have been reduced considerably.

465 In Fig. 7 the prompt index values were downloaded from the web portal http://pcindex.org in near-
466 real time, while the post-event (final) index values were downloaded at a much later time. For
467 further comparisons of IAGA-endorsed methods with the present DMI calculation scheme, Fig. 10
468 presents for the same dates real-time values of PCN and PCS, which have been constructed from
469 past data using HSRW QDC values on pre-event data only, while the post-event (final) PCN and
470 PCS values have been derived by using the full ±40 days SRW-QDCs.
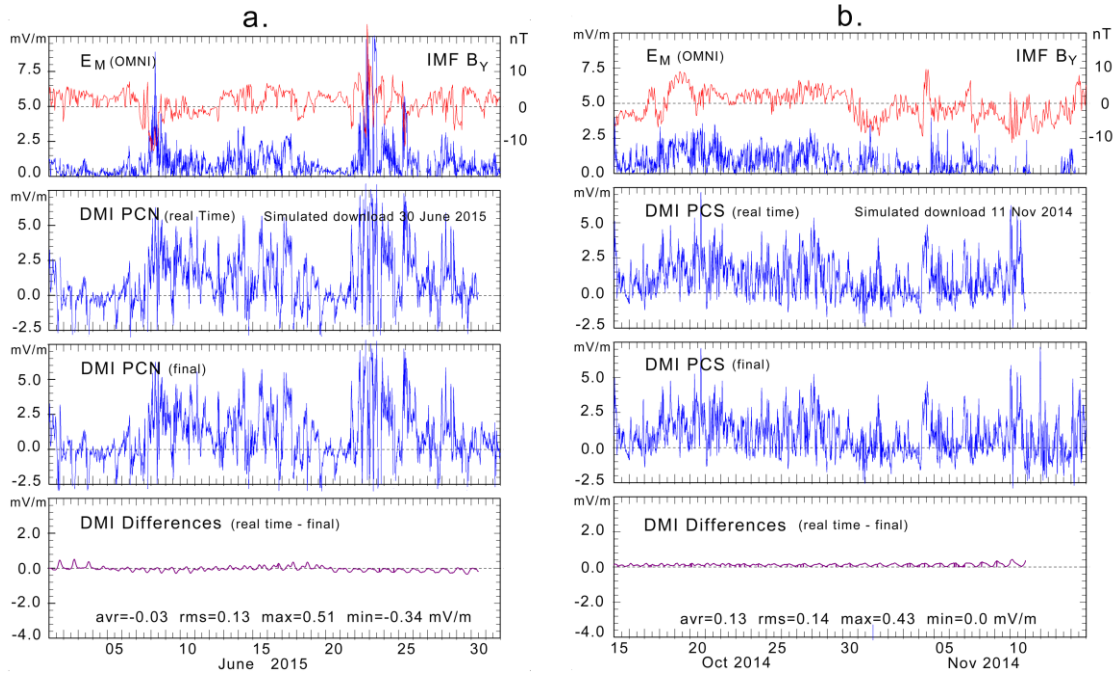
Figure 10. PCN and PCS real-time 15-min values calculated for simulated downloads by using pre-event data only in HSRW QDCs. PCN and PCS final values were calculated by using full SRW QDCs.

Comparing the differences between prompt and post-event PC index values in Fig. 10 with those displayed in Fig. 7 demonstrates the strongly reduced differences obtained by using the HSRW QDC derivation scheme instead of the IAGA-endorsed cubic spline extrapolation method.

An example of both the reduced differences between real-time and final PC index values and the increased robustness to missing data with the DMI method compared to the IAGA-endorsed method is shown in Fig. 11 from Stauning (2018c). The calculations are based on Qaanaaq (THL) data from 2015, which were exposed to irregular recordings at the end of July.
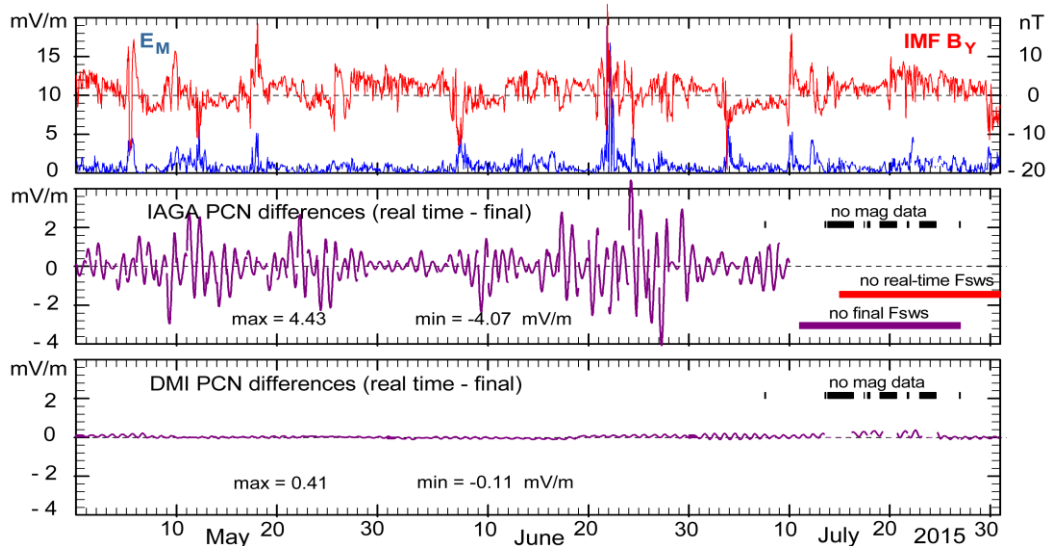
Figure 11. Differences between PCN hourly index values calculated by using real-time and final values of F_{SWS} in the IAGA-endorsed versions in the middle field and the corresponding differences for the PCN indices in the DMI versions in the bottom field. Intervals of missing values are marked in both lower fields. (from Stauning, 2018c).

487 PCN index values could not (of course) be calculated where data are missing. The reference levels
488 in the IAGA-endorsed versions are strongly affected by the missing or corrupted median values
489 throughout intervals extending beyond the sections of missing data. The "IAGA PCN differences"
490 of up to more than 4 mV/m in Fig. 11 have been calculated from solar sector terms derived by using
491 the procedure defined in J&T2011.

492 For Space Weather applications the risk of false PC index values caused by missing data throughout
493 parts of the days, which may cause large displacements of their median values, is probably still
494 more important than missing index data. In an example discussed in Stauning (2018c), where data
495 were made unavailable for 12 hours, the post-event PC index values were changed significantly
496 throughout 13 days centred at the disturbed day. The near-real time indices were changed
497 throughout 8 days after the disturbance by up to 4 mV/m occurring 2 days after the interval of
498 unavailable data. Such amounts may falsely indicate (or hide) strong magnetic storm conditions
499 without warnings.

500 In Fig. 11, the "DMI PCN differences" between real-time and final PCN index values in the
501 versions based on the SRW techniques remain small (below 0.5 mV/m) and almost unaffected by
502 intervals of missing data. In addition, and of prime importance for the potential use of real-time PC
503 indices in Space Weather monitoring, the SRW-based QDC method, as evident from Fig. 11, is far
504 more robust to data supply irregularities than the cubic spline-based forward extrapolation
505 technique that depends critically on the completeness of data samples.

506 The application of the DMI methods defined in Stauning (2016), to derive real-time and final PC
507 index values from polar magnetic data assumed currently available, is detailed in the appendix to
508 Stauning (2018c). Relevant magnetic data might be obtained for qualified PCN and PCS
509 calculations from further observatories in the central Polar Regions like Resolute Bay and Dome-C
510 beyond the standard observatories, Qaanaaq and Vostok.

511

512

7. Discussions

514 It should be stressed that the median-based reference levels used in the IAGA-endorsed versions are
515 not quiet levels and thus differ from previous real or verbal definitions of the PC index reference
516 level in publications included those listed as supporting references in the IAGA endorsement
517 documentation written by Matzka (2014) (e.g., Troshichev et al., 2006; Janzhura and Troshichev,
518 2008; Troshichev, 2011; Janzhura and Troshichev, 2011, Troshichev and Janzhura, 2012a;
519 Troshichev and Janzhura, 2012b). Even at the web portal (http://isgi.unistra.fr) of the International
520 Service of Geomagnetic Indices, ISGI, the PC index definition states (incorrectly) that index values
521 are derived from deviations from the quiet level. The use of median-based reference levels has
522 never been validated in publications and must be considered based on an unjustified postulate
523 originating in Menvielle et al. (2011) and further specified in Janzhura and Troshichev (2011).

524 A main objection against the IAGA-endorsed reference level construction is the resulting local time
525 variation in IMF B_Y-related effects seen in the H-QDC component in Fig 3 or in the effects on the
526 PCN index values seen in Fig. 4. In both cases the IMF B_Y-related effects contrary to anticipated
527 principles maximize at local night when the observatory is farthest apart from the Cusp region
528 where the IMF By-related effects originate.

529 It is not, of course, questioned here that the IMF B_Y conditions significantly affect the polar
530 convection patterns and related magnetic variations. However, for the median-based reference level
531 construction, the assumption that slowly varying IMF B_Y levels would not affect geomagnetic
532 disturbance conditions has never been validated and may be incorrect in the complicated interplay

533 between the IMF B_Y- and B_Z- related effects. A further questionable feature in the reference level
534 derivation method is the implied assumption that SWS terms calculated from daily median values
535 could be applied to remove solar wind sector effects throughout the whole day disregarding the
536 variations in the IMF B_Y–related effects with the varying observatory position in the polar cap. The
537 real IMF B_Y-related SWS effects on the PC indices could even be opposite of the constructed
538 effects resulting from using reference level values derived by the median-based methods whether in
539 the post-event or in the real-time version.

540 The example PCN calculations displayed in Fig. 4 were based on the case presented in J&T2011
541 with a smoothed IMF B_Y value of 4 nT, which is not uncommon. Unjustified SWS contributions of
542 3-4 mV/m could be expected for the stronger cases (larger IMF B_Y). Such magnitudes are around
543 twice the onset level of around 2 mV/m for magnetic storm or substorm activity (Troshichev et al.,
544 2014), which definitely makes the IAGA-endorsed "final" PCN indices unsuitable for scientific
545 applications.

546 For the PCS indices, corresponding problems with the post-event reference levels may exist in spite
547 of the statement in p. 1492-1493 of J&T2011 that SWS effects are negligible at Vostok on the
548 Antarctic ice cap. It has not been possible to obtain a description of the present PCS calculation
549 methods from the index provider (AARI) or from the index publisher (ISGI) for further examination
550 of this issue.

551 For the real-time PCN and PCS indices, the excessive excursions in the cubic-spline extrapolated
552 reference levels may generate unfounded differences between near-real time and post-event index
553 values of more than 4 mV/m. Such excursions with magnitudes at magnetic storm levels make the
554 near-real time IAGA-recommended PC indices unreliable and thus unsuitable for Space Weather
555 monitoring and related research. Their strong vulnerability to intervals of incomplete data with the
556 maximum adverse effects appearing two days after the occurrence of data irregularities is an
557 additional invalidating feature to be considered.

558 It has not been possible to obtain descriptions of the real-time PCN and PCS calculation methods
559 from the index provider (AARI) or from the index publisher (ISGI). It has also not been possible to
560 obtain archived recordings of near-real time PCN and PCS indices provided to the community
561 through the AARI web portal http://pcindex.org and the ISGI web site http://isgi.unistra.fr .

562 The concerns over the inconsistent index derivation methods and lack of documentation have been
563 forwarded to IAGA Executive Committee, Index Task Force and Working Group representatives
564 and to the PC index providers at AARI and DTU Space with suggestions for thorough analyses of
565 PC index calculation methods. The specific concerns have not been responded to and the
566 suggestions for further analyses of the index derivation methods have been rejected so far.

567

8. Irregular PCS excursions

569 The search for unjustified SWS effects in the PC index series has disclosed numerous examples of
570 irregular unjustified PCS excursions. An example from a recent download of PCN and PCS data
571 from 15-18 December 2011 is displayed in Fig.12 (For the review process, further examples from
572 still more recent downloads (27 Jan 2020) are shown in appendix A2.)

573 Fig. 12 displays in addition corresponding PCN and PCS values derived by the DMI index
574 procedure (Stauning, 2016). The display of PCS index values based on Vostok data is supplemented
575 by PCS index values derived from Dome-C (DMC) magnetic data, which are of very good quality.
576 The Vostok and Dome-C data generate nearly identical PCS values and indicate very low
577 disturbance levels. The interval is very quiet (Kp values between 0 and 1) which is also evident
578 from the PCN data in both versions.
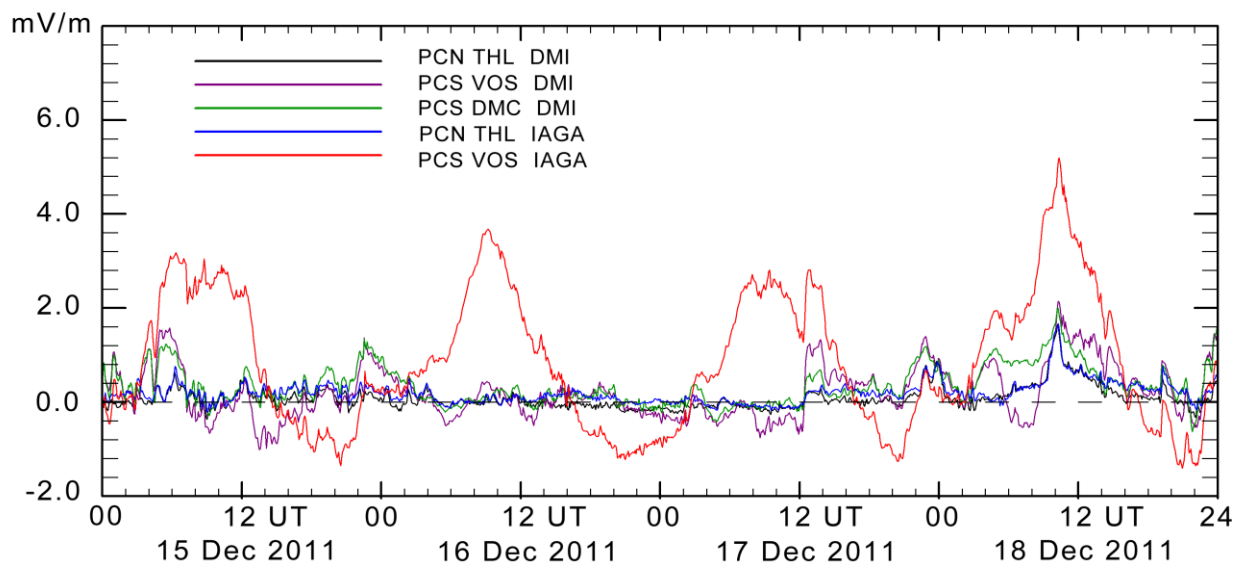
Figure 12. Display of published PCN (blue line) and PCS (red) values from 15-18 December 2011. PCN (black) from Qaanaaq data, PCS from Vostok (magenta) and Dome-C (green) data derived by a different method (DMI, Stauning, 2016) have been added to the diagram.

It is easy to see that the published Vostok PCS data have unjustified daily variations between -1.5 and up to +4.0 mV/m (a level indicative of strong magnetic storm conditions). The additional top of 1 mV/m bringing the PCS value up to 5.0 mV/m at 11 UT on 18 December is probably a real event. The Vostok magnetic data supplied from INTERMAGNET are final values.

The excessive PCS variations are probably not caused by implementation of the SWS-related reference level construction but may have resided in the PCS index values calculated at AARI throughout the years and brought to attention now by the recent examination of PCS data for SWS effects. The PCS index failure is mentioned here to underline the point that PC index series need careful monitoring and evaluation of index quality, which is apparently not implemented.

Information on the problem in the PCS index series distributed from ISGI (http://isgi.unistra.fr) and the AARI index web portal (http://pcindex.org) was published in Stauning (2018b) and also sent directly to the index providers and to ISGI and IAGA representatives in 2018. Their only reaction – so far – has been to state that the published PCS index data are just provisional values to be applied to scientific works at users own risk (communication from IAGA Executive Committee, 21 May 2018).

Conclusions.

- The Polar Cap indices in their real-time versions have the potential to become very important tools for Space Weather monitoring and forecasts and in their final versions important for Space Weather-related research. However, the presently published PCN and PCS index series are considered invalid.

- The published series of (nominally) final PCN index values calculated by the methods endorsed by IAGA may include unjustified contributions of up to 3-4 mV/m just due to the handling of IMF B_Y-related solar wind sector effects in the reference level construction. An example case gave unjustified contributions of up to 2.5 mV/m (magnetic storm level) to PCN index values. Such unjustified contributions are considered to make the "final" PCN index series invalid.

609 - The series of near-real time PCN and PCS index values calculated by the methods endorsed by
610 IAGA may display considerable differences with respect to their corresponding post-event values.
611 An example case using the referenced calculation procedures to the letter gave differences of up to
612 2.8 mV/m for a moderate event. Further examples of calculations of effects have given differences
613 of more than 4 mV/m. At occasional downloads of near-real time index values and comparison to
614 later downloads of final values, differences of up to 3.7 mV/m have been documented in cases not
615 particularly extreme.

616 - The IAGA-endorsed near-real time index calculation method based on cubic spline extrapolation
617 of past median values is extremely vulnerable to irregularities in the data supply. An example of 12
618 hours of missing data gave unfounded excursions of up to 4 mV/m two days later. Such excursions
619 may falsely indicate (or hide) strong magnetic storm conditions and are considered to make the
620 IAGA-recommended near-real time indices highly unreliable and thus unsuitable for Space Weather
621 applications.

622 - The provisional PCS index series, which is not approved by IAGA but still made available from
623 ISGI and used in the scientific community, displays unexplained erroneous excursions of up to 4
624 mV/m in the recorded examples shown here. Final magnetic data were available for the index
625 examples and the IAGA-endorsed calculation methods were probably used. Similar or even larger
626 undetected excursions are possible. The example underlines the need for careful examination of
627 index quality in the published PC index series.

628 - It is suggested that IAGA should initiate a careful evaluation of present index series and index
629 derivation methods and ensure that full documentation of the presently applied index calculation
630 procedures is made available in agreement with its *Criteria for endorsement of indices by IAGA,*
631 *sec.2* (2009). Presently, there is no available documentation of present PCS index derivation
632 procedures or of the near-real time PCN and PCS calculation methods.

633 - On basis of the problems reported here, IAGA might consider encouraging developments of
634 improved PC index calculation methods. Alternative more accurate and reliable methods are
635 available.

636

637 **Data availability:**

638 Near real-time (prompt) PC index values and archived PCN and PCS index series derived by the
639 IAGA-endorsed procedures are available through AARI and ISGI web sites. Archived PCN and
640 PCS data used in the paper were downloaded from http://pcindex.org on 15 November 2019 unless
641 otherwise noted. The web site, furthermore, holds PCN and PCS index coefficients, whereas QDC
642 and SWS values are not included. The web site includes the document "Polar Cap (PC) Index"
643 (Troshichev, 2011).

644 It is presently not known (in spite of requests) whether the near real-time PC index suppliers (AARI
645 and ISGI) retain copies of the published values. If not available from the index suppliers, then
646 values of occasionally downloaded values held by the author could be delivered, for instance, in
647 their original (zip-encoded) formats to a data repository or included in a data supplement.

648 Geomagnetic data from Qaanaaq, Vostok, and Dome-C were supplied from the INTERMAGNET
649 data service web portal at http://intermagnet.org.

650 The observatory in Qaanaaq is managed by the Danish Meteorological Institute, while the
651 magnetometer there is operated by DTU Space, Denmark. The Vostok observatory is operated by
652 the Arctic and Antarctic Research Institute in St. Petersburg, Russia. The Dome-C observatory is

References

667   Chun, F. K., Knipp, D. J., McHarg, M. G.., Lu, G., Emery, B. A., Vennerstrøm, S., Troshichev, O.
668   A. (1999), Polar cap index as a proxy for hemispheric Joule heating, *Geophys. Res. Lett.*, *26* ,
669   1101-1104. https://doi.org/10.1029/1999GL900196

670   Chun, F.K., Knipp, D. J., McHarg, M. G., Lacey, J. R., Lu, G., and Emery, B. A. (2002), Joule
671   heating patterns as a function of polar cap index, *J. Geophys. Res*., *107* (A7),
672   https://doi.org/10.1029/2001JA000246 .

673   Iijima, T., Potemra, T.A. (1976). Field-aligned currents in the Cusp observed by Triad, *Journal of*
674   *Geophysical Research*, 81, 5971-5979. https://doi.org/10.1029/JA081i034p05971

675   IAGA Resolution no. 3 (2013): http://www.iaga-aiga.org/resolutions.

676   IAGA Index endorsement criteria (2009):
677   https://www.ngdc.noaa.gov/IAGA/vdat/GeomagneticIndices/Criteria_for_Endorsement.pdf

678   Huang, C.-S. (2005), Variations of polar cap index in response to solar wind changes and
679   magnetospheric substorms, *J. Geophys. Res.*, 110, A01203,
680   https://doi.org/10.1029/2004JA010616 .

681   Janzhura, A. S., Troshichev, O. A. (2008). Determination of the running quiet daily geomagnetic
682   variation. *Journal of Atmospheric and Solar-Terrestrial Physics,* 70, 962–972.
683   https://doi.org/10.1016/j.jastp.2007.11.004 .

684   Janzhura, A. S., Troshichev, O. A. (2011). Identification of the IMF sector structure in near-real
685   time by ground magnetic data. *Annales Geophysicae,* 29, 1491-1500.
686   https://doi.org/10.5194/angeo-29-1491-2011 .

687   Janzhura, A. S., Troshichev, O. A., Stauning, P. (2007). Unified PC indices: Relation to the isolated
688   magnetic substorms. *Journal of Geophysical Research,* 112, A09207.
689   https://doi.org/10.1029/2006JA012132 .

690   Kan, J. R., Lee, L. C. (1979). Energy coupling function and solar wind-magnetosphere dynamo.
691   *Geophysical Research Letter,* 6 (7)**,** 577– 580. https://doi.org/10.1029/GL006i007p00577 .

692   Liou, K., Carbary, J. F., Newell, P. T., Meng, C. I., and Rasmussen, O. (2003). Correlation of
693   auroral power with the polar index, *J. Geophys. Res.*, *108* (A3), 1108,
694   https://doi.org/10.1029/2002JA009556 .

695   Matzka, J. (2014). PC_index_description_main_document_incl_Appendix_A.pdf. Available at
696   DTU Space web portal: ftp://ftp.space.dtu.dk/WDC/indices/pcn/

697   Menvielle, M., Iyemori, T., Marchaudon, A., Nosé, M. 2010. Geomagnetic Indices. Ch.8 in: M.
698   Mandea, M. Korte (eds), *Geomagnetic Observations and Models*, IAGA Special Sopron Book
699   Series 5, 2011. pp.183-228. https://doi.org/10.1007/978-90-481-9858-0_8

700   Nagatsuma T. (2002). Saturation of polar cap potential by intense solar wind electric fields,
701   *Geophys. Res. Let.*, *29*, (10), 621. https://doi.org/10.1029/2001GL014202

702   Nielsen, J. B. and Willer, A. N. (2019). Restructuring and harmonizing the code used to calculate
703   the Definitive Polar Cap Index, *Report from DTU Space*. https://tinyurl.com/sx3g5t5

704   Ridley A.J. and Kihn, E. A. (2004). Polar cap index comparisons with AMIE cross polar cap
705   potential, electric field, and polar cap area, *Geophys. Res. Lett.*, *31*, L07801,
706   https://doi.org/10.1029/2003GL019113 .

707   Stauning, P. (2011). Determination of the quiet daily geomagnetic variations for polar regions, *J.
708   Atmos. Solar-Terr. Phys.*, https://doi.org/10.1016/j.jastp.2011.07.004 .

709   Stauning, P. (2012). The Polar Cap PC Indices: Relations to Solar Wind and Global Disturbances,
710   Exploring the Solar Wind, Marian Lazar (Ed.). *InTech Publ.*. ISBN: 978-953-51-0339-4.
711   https://doi.org/10.5772/37359

712   Stauning, P. (2013a). The Polar Cap index: A critical review of methods and a new approach, *J.
713   Geophys. Res. Space Physics*, 118, 5021-5038. https://doi.org/10.1002/jgra.50462

714   Stauning, P. (2013b). Comments on quiet daily variation derivation in "Identification of the IMF
715   sector structure in near-real time by ground magnetic data" by Janzhura and Troshichev (2011).
716   *Annales Geophysicae,* 31, 1221-1225. https://doi.org/10.5194/angeo-31-1221-2013 .

717   Stauning P. (2013c). Power grid disturbances and polar cap index during geomagnetic storms, *J
718   Space Weather Space Clim*. *3*: A22. https://doi.org/10.1051/swsc/2013044 .

719   Stauning, P. (2015). A critical note on the IAGA-endorsed Polar Cap index procedure: effects of
720   solar wind sector structure and reverse polar convection. *Annales Geophysicae,* 33**,** 1443-1455.
721   https://doi.org/10.5194/angeo-33-1443-2015 .

722   Stauning, P. (2016). The Polar Cap (PC) Index.: Derivation Procedures and Quality Control. *DMI
723   Scientific Report SR-16-22*. Available at:
724   https://www.dmi.dk/fileadmin/user_upload/Rapporter/TR/2016/SR-16-22-PCindex.pdf .

725   Stauning, P. (2018a). A critical note on the IAGA-endorsed Polar Cap (PC) indices: excessive
726   excursions in the real-time index values. *Annales Geophysicae,* 36, 621–631.
727   https://doi.org/10.5194/angeo-36-621-2018 .

728   Stauning, P. (2018b): Multi-station basis for Polar Cap (PC) indices: ensuring credibility and
729   operational reliability. *Journal of Space Weather and Space Climate,* 8, A07.
730   https://doi.org/10.1051/swsc/2017036 .

731   Stauning, P. (2018c). Reliable Polar Cap (PC) indices for space weather monitoring and forecast,
732   *Journal of Space Weather and Space Climate,* 8**,** A49. https://doi.org/10.1051/swsc/2018031

733   Stauning, P. (2020). Using PC indices to predict violent GIC events threatening power grids.
734   *Journal of Space Weather and Space Climate*. https://doi.org/10.1051/swsc/202004 .

735   Stauning, P., Troshichev, O. A., and Janzhura, A. S. (2008). The Polar Cap (PC) index: Relations to
736   solar wind parameters and global activity level, *J. Atmos. Solar-Terr. Phys.*,
737   https://doi.org/10.1016/j.jastp.2008.09.028 .

Troshichev, O. A. (2011). Polar Cap (PC) Index. Available at: http://pcindex.org (see Supported materials).Troshichev, O. A. and Andrezen, V. G. (1985). The relationship between interplanetary quantities and magnetic activity in the southern polar cap. *Journal of Planetary and Space Science*, 33, 415-419. https://doi.org/10.1016/0032-0633(85)90086-8

Troshichev, O. A. and Janzhura, A. S. (2012a). Physical implications of discrepancy between summer and winter PC indices observed in the course of magnetospheric substorms. *Advances in Space Research,* 50 (1), 77-84. https://doi.org/10.1016/j.asr.2012.03.017

Troshichev, O. A. and Janzhura, A. S. (2012b). Space Weather monitoring by ground-based means, *Springer Praxis Books*. Heidelberg. https://doi.org/10.1007/978-3-642-16803-1 .

Troshichev, A. O. and Lukianova, R. Y. (2002). Relation of PC index to the solar wind parameters and substorm activity in time of magnetic storms, J. Atmos. Solar-Terr. Phys., 64, 585. https://doi.org/10.1016/S1364-6826(02)00016-0 .

Troshichev, O. A., Sormakov, D. A. (2017). PC index as a proxy of the solar wind energy that entered into the Magnetosphere: 3. Development of magnetic storms, *J. Atmos. Solar-Terr. Phys.* https://doi.org/10.1016/j.jastp.2017.10.012

Troshichev, O. A., Andrezen, V. G., Vennerstrøm, S., Friis-Christensen, E. (1988). Magnetic activity in the polar cap – A new index. *Journal of Planetary and Space Sciences*, 36(11), 1095-1102. https://doi.org/10.1016/0032-0633(88)90063-3

Troshichev, O. A., Janzhura, A. S., Stauning, P. (2006). Unified PCN and PCS indices: method of calculation, physical sense and dependence on the IMF azimuthal and northward components. *Journal of Geophysical Research,* 111, A05208. https://doi.org/10.1029/2005JA011402 . (note correction in Troshichev et al., 2009)

Troshichev, O. A., Janzhura, A. S., Stauning, P. (2009). Correction to "Unified PCN and PCS indices: Method of calculation, physical sense, and dependence on the IMF azimuthal and northward components", *Journal of Geophysical Research*, 114, A11202. https://doi.org/10.1029/2009JA014937 .

Troshichev, A. O., Lukianova, R. Y., Papitashvili, V. O., Rich, F. J. and Rasmussen, O. (2000). Polar Cap index (PC) as a proxy for ionospheric electric field in the near-pole region, Geophys. Res. Lett., 27, 3809. https://doi.org/10.1029/2000GL003756

Troshichev, O. A. , Podorozhkina, N. A., Sormakov, D. A., Janzhura, A. S. (2014). PC index as a proxy of the solar wind energy that entered into the magnetosphere: 1. Development of magnetic substorms. *Journal of Geophysical Research, Space Physics,* 119. https://doi.org/10.1002/2014JA019940 .

Vassiliadis, D., V. Angelopoulos, D. N. Baker, A. J. Klimas (1996), The relation between the northern polar cap and auroral electrojet geomagnetic indices in the wintertime, *Geophys. Res. Lett*., *23*, 2781. https://doi.org/10.1029/96GL02575 .

Vennerstrøm, S. (1991). The geomagnetic activity index PC, PhD Thesis, Scientific Report 91-3, Danish Meteorological Institute, 105 pp. https://www.dmi.dk/fileadmin/user_upload/Rapporter/SR/1991/sr91-3.pdf

Vennerstrøm, S., Friis-Christensen, E., Troshichev, O. A., Andrezen, V. G. (1991). Comparison between the polar cap index PC and the auroral electrojet indices AE, AL and AU, *J. Geophys. Res.*, *96*, 101. https://doi.org/10.1029/90JA01975

Wilhjelm, J., Friis-Christensen, E., Potemra, T. A. (1972). The relationship between ionospheric and field-aligned currents in the dayside cusp, J. Geophys. Res. 83, 5586. https://doi.org/10.1029/JA083iA12p05586

783

786

Conflict of interest:

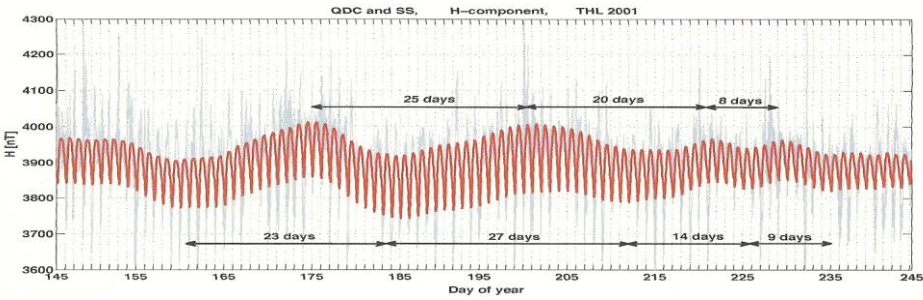I have no conflict of interest

789

790   **Appendix A1** (This appendix is intended for the review process only.)

791   **A1-1. Reference level**. The only published description of real-time versions of the Polar Cap (PC) indices,
792   PCN and PCS, is found in Janzhura and Troshichev (2011): Identification of the IMF sector structure in
793   near-real time by ground magnetic data (J&T2011) (and its replicate in Troshichev and Janzhura, 2012,
794   T&J2012). The publication holds (p.1496) a step-by-step procedure for the calculation of IMF By-related
795   solar wind sector (SWS or SS) terms by forward cubic spline-based extrapolation of past median values. The
796   SS terms are used in the derivation of reference levels for measuring magnetic variations. In their work, in
797   spite of statements to the opposite, there are no examples of near-real time data or values derived from using
798   the specified real-time method.

799   The present note provides copies of figures of J&T2011 (T&J2012), and displays corresponding figures
800   based on post-event as well as real-time data processing at DMI.

801

Fig. A1-1. PCN reference level (red) superimposed on recorded H-component data. From Fig. 1 of J&T2011, reproduced here in colour from Fig. 4.10 of T&J2012

Figure 4.10 The actual variation of 1-min values of the geomagnetic *H* component at Thule station in the summer season of 2001 (blue thin line) and superposed quiet daily curve (QDC) characterizing the daily variation of the quiet geomagnetic field (red thick line).
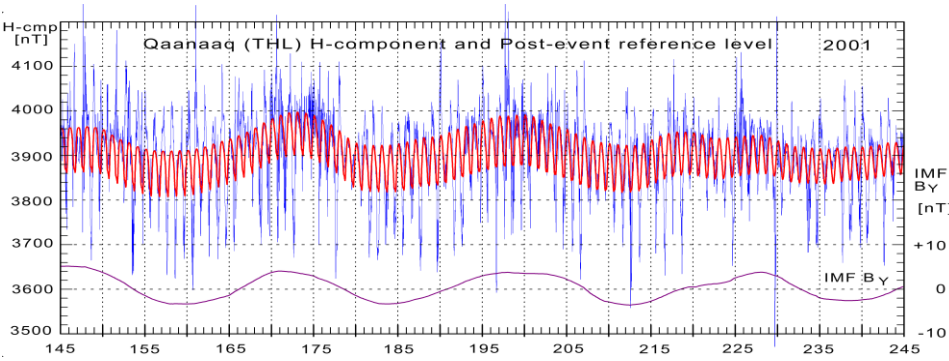
Fig. A1-2. PCN post-event (final) reference level values (red line) supplied from DTU Space superimposed on recorded H-component data. IMF By values added.
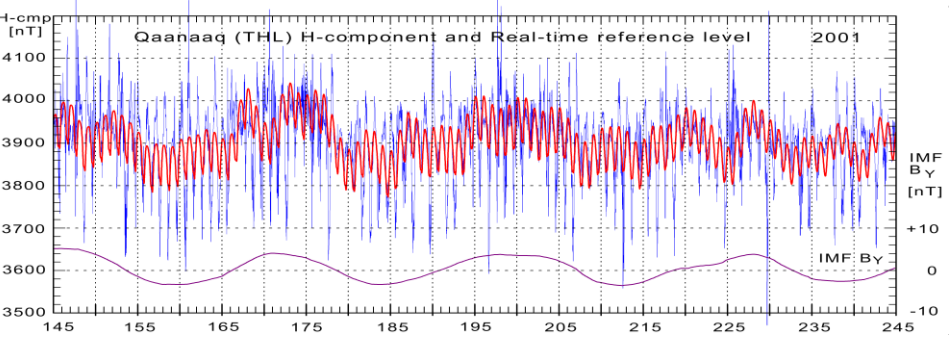
Fig. A1-3. PCN real-time reference level (red) derived by using J&T2011 procedure to the letter. Recorded H-component data. IMF By values added.

809   The close similarity of the reference level (red line) in Fig.A1-1 with that of Fig.A1-2 and the strong
810   difference with respect to the real-time reference level in Fig.A1-3 implies that the "QDC" in Fig.A1-1 was
811   actually derived by post-event (final) calculation methods like those used for Fig.A1-2.

812

813   **A1-2. Solar Wind Sector (SS) term.**
814   The IMF By-related solar wind sector effects on the convection patterns generate changes in the PC index
815   response to the merging electric fields. A solar wind sector term was first suggested by Menvielle et al.
816   (2011) and implemented in the derivation of PC index reference levels by Janzhura and Troshichev (2011)
817   (replicated in T&J2012). For post-event processing the SS terms were derived as the smoothed average
818   values of 7 days daily median values. For real-time processing, the SS terms are derived from cubic spline-
819   based extrapolation of past median values according to J&T2011 (T&J2012). However, in spite of the
820   explicit statement in p. 1496 of J&T2011 assuring that the illustration of the SS term in their Fig. 6 (Fig. 4.15
821   in T&J2012) is based on using the real-time procedure, the figure actually presents values derived by the
822   post-event method (7-days smoothed average daily medians).
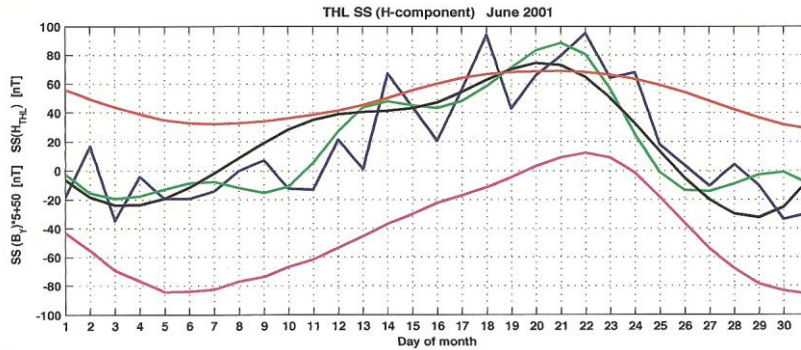
Fig. A1-4. THL H-component. 1-day (blue), 3-days (green) and 5-days (black) median values. H_{SS} terms in magenta line on scale shifted 50 nT downward for clarity. Smoothed IMF By multiplied by 5 and shifted 50 nT upward. (From Fig. 6 of J&T2011. Here copied from Fig. 4.15 of T&J2012)

823

Figure 4.15 Behavior of the median values of the magnetic *H* component at Thule station during June months of 1998 (a) and 2001 (b) for intervals with duration of 1 day (blue line), 3 days (green line), and 5 days (black line). The red line shows the variation of the IMF B_y component, derived from spacecraft measurements. The magenta line shows the variation reconstructed from geomagnetic *H* component. To be clearly demonstrated the actual B_y values were multiplied by a five and were shifted by 50 nT to a higher position, whereas the curve of reconstructed *H* component was shifted by 50 nT to a lower position.

824
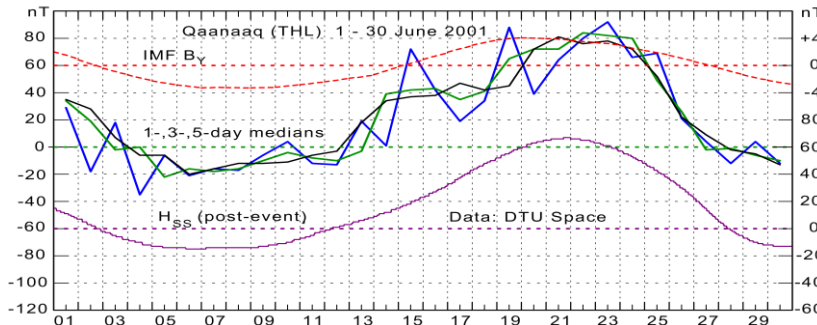
Fig. A1-5. THL 1-, 3-, 5-day medians on left scale. Post-event H_{SS} terms are displayed in magenta line on lower right scale. Data were supplied from DTU Space. IMF By values added on upper right scale (OMNI).

825
826
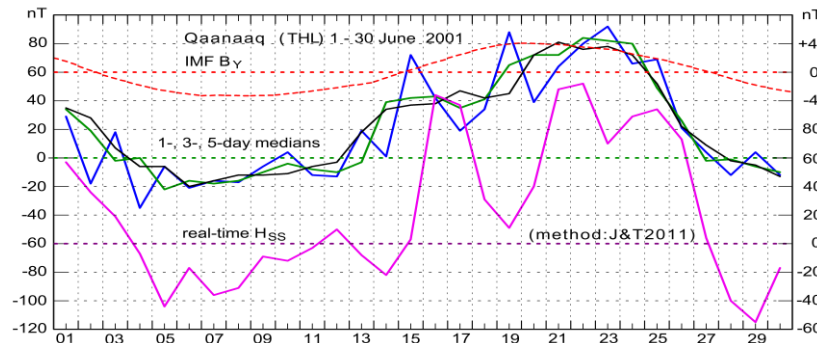
Fig. A1-6. THL 1-, 3-, 5-day medians on left scale. Real-time H_{SS} terms in magenta line on lower right scale. H_{SS} values were calculated by following the procedure in J&T2011 to the letter. IMF By added on upper right scale

827
828

829   The similarity between the H_{SS} curves in Figs.A1-4 and A1-5 and the large difference with respect to the
830   real-time H_{SS} values in Fig.A1-6 implies that the display in Fig. 6 of J&T2011 (Fig. 4.15 of T&J2012),
831   contrary to the statement in p. 1496, was actually generated from using post-event calculations.
832

833 **A1-3. H-component and SS terms.**

834 Fig. 7 in J&T2011 (Fig. 4.16 in T&J2012) displays the H-component recorded at Qaanaaq (THL) throughout
835 year 2001. The IMF B_Y-related H_{SS} values have been superimposed on the recordings. The black asterisks
836 are supposed to present real-time, the red asterisks present post-event values.
837

838
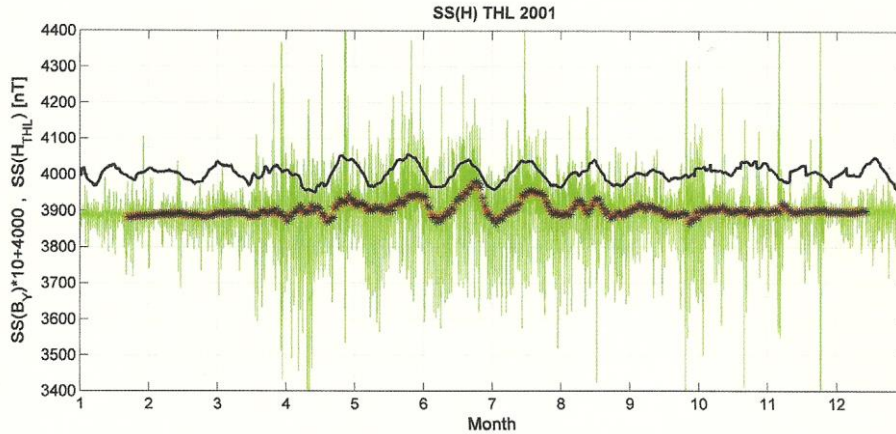
Fig. A1-7. Presentation of one year's THL H-component data (green line) with superimposed real-time (black), and post-event H_{SS} values (red asterisks). IMF By values added (black line). From Fig. 7 of J&T2011. Here copied from Fig.4.16 of T&J2012

Figure 4.16 The SS effects derived in the *H* component observed at station Thule in 1998 (a) and 2001 (b). The actual variation of the ground *H* component is shown by a green line, whereas black asterisks present the SS structure obtained by the extrapolation procedure when all data are available until the examined day (n=1); and red asterisks present the interpolated SS structure derived under the condition that the examined day is in the middle of the gap in the time interval. The actual variation of the IMF B_y component values measured by ACE spacecraft were multiplied by a ten and were shifted by 4000nT to a higher position (thin black line).

839
840
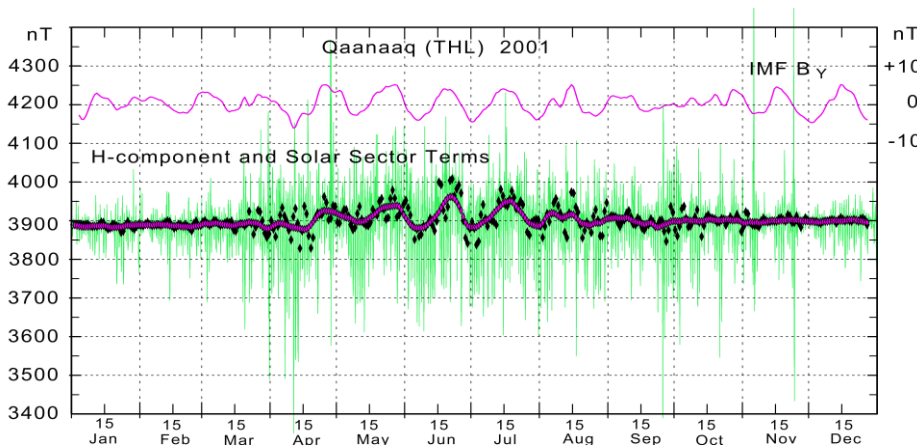
Fig. A1-8. THL H-component data with superimposed real-time (black), and post-event (red diamonds) values of H_{SS}. Note the large scatter of the real-time (black) diamonds. IMF By values added.(red line) on upper right scale.
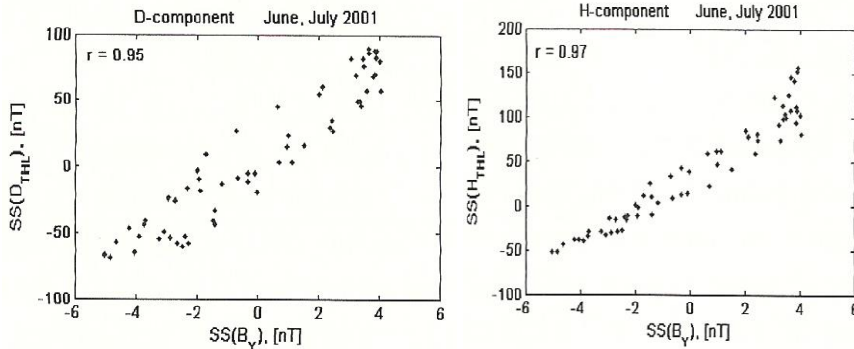
841
842
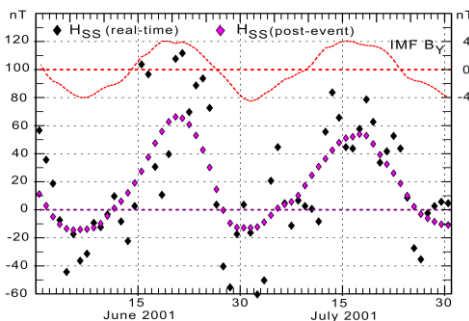
Fig. A1-9. Detailed plot of June-July section of Fig. A8. Black diamonds present real-time H_{SWS} values derived by using the J&T2011 procedure (p.1496) to the letter. The magenta diamonds present post-event (final) H_{SS} values supplied from DTU Space. They represent daily median H-component values averaged and smoothed over 7 days at a time. IMF B_y values displayed in red line on right scale.

843
844

845 It is evident from Figs.A1-8 and A1-9 that the real-time and post-event methods generate quite different
846 values of the IMF B_Y-related solar wind sector terms, H_{SS}. The red set of asterisks in Fig. A1-7, no doubt,
847 present post-event values, while the black set, against the statement in the caption, could not present real-
848 time values.

849 **A1-4. SS term vs. IMF By**

850 From the post-event processing it appears that the H- and D-solar wind sector terms are highly correlated
851 with the daily mean IMF B_Y values. Thus, they could be used to estimate past IMF B_Y levels and signs with
852 good probability. However, according to the title and abstract of the publication, "Identification of the IMF
853 sector structure in near-real time by ground magnetic data", the real-time and not the post-event option is the
854 target.
855

856

Fig. A1-10. Fig. 8b from J&T2011 (Fig.4.17 from T&J2012).Relations between daily average IMF B_Y values and solar wind sector D_{SS} and H_{SS} values. H_{SS} scale values are too large by a factor 2 (cf. their Fig. 4.16).

Figure 4.17 Relationship between the sector structure magnitudes derived by satellite-based and ground-based sets of magnetic data for summer months of 1998 (upper row) and 1991 (lower row). Geomagnetic D (left column) and H (right column) components at the Thule stations were analyzed.

Year 1991 should be 2001.

857
858

859
860
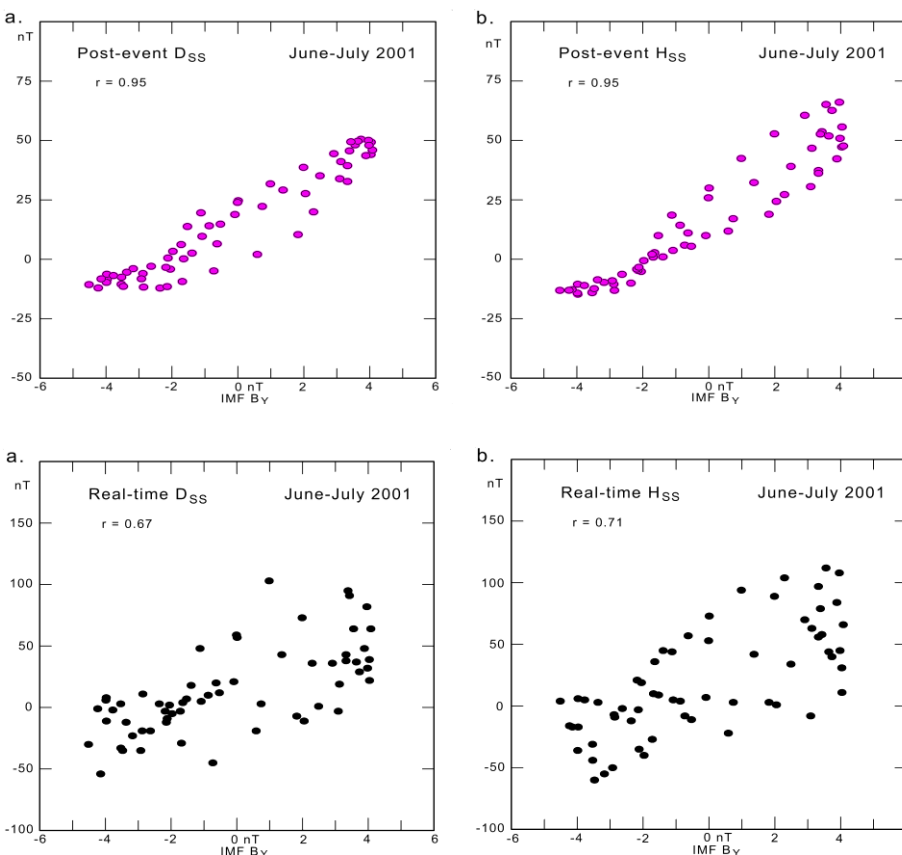
Fig. A1-11. Display of post-event (final) solar wind sector terms, H_{SS}, supplied from DTU Space vs. daily average IMF B_Y values. Note the H_{SS} scales differ by factor 2 from those of Fig. A10, i.e., Fig. 8 of J&T2011 (Fig. 4.17 of T&J2012).

Fig. A1-12. Display of real-time solar wind sector terms, H_{SS}, calculated by using the procedure in J&T2011, p.1496, to the letter, plotted vs. daily average IMF B_Y values.

861
862
863 Contrary to the D_{SS} and H_{SS} solar wind sector terms derived by post-event calculations displayed in Figs. A1-
864 10 and A1-11, the corresponding solar wind sector terms generated by using real-time processing are less
865 well correlated with the daily average IMF B_Y values. The relation displayed by the scattered values in Fig.
866 A1-12 could hardly be used to determine the actual IMF By magnitude level and sign with certainty.

867

A1-5. Appendix A1 summary.

With the title of the publication, Janzhura and Troshichev (2011) (or its replica in section 4.4 of Troshichev and Janzhura, 2012): "*Identification of the IMF sector structure in near-real time by ground magnetic data*" and their abstract: "*A method is proposed to determine in near-real time the interplanetary magnetic field (IMF) sector structure effect on geomagnetic data from polar cap stations*", the publication could be expected to present examples of near-real time data or derived results.

The publication presents the IMF By-related solar wind sector effects by introducing solar wind sector terms (D_{SS} and H_{SS}) derived from the daily median component values averaged throughout 7 days with the day of interest at the middle. These solar wind sector terms are used for calculations of the reference level from which the polar magnetic disturbances used to generate the polar cap (PC) indices are derived (Matzka, 2014).

The post-event method was extended to generate solar wind sector terms in near-real time by cubic spline-based extrapolation of past median values using the procedure specified in p.1496 of J&T2011 (p.62 of T&J2012). It appears that this procedure has actually been used since then to generate the near-real time PC index values presented at the AARI web portal (http://pcindex.org) and the ISGI web site (http://isgi.unistra.fr). These PC index values have been shown to display excessive excursions with respect to the corresponding post-event (final) index series (Stauning, 2018a).

In spite of specific statements to the opposite, neither Fig. 6 nor Fig. 7 of J&T2011 (Figs. 4.15 and 4.16 of T&J2012) present near-real time values of the solar wind sector terms. They both, most likely, present values derived by post-event methods as inferred from Figs. A4-A9 of this appendix.

Actually, none of the 8 figures in J&T2011 (T&J2012) displays near-real time values or derived results. Figs. 1, 6, 7, and 8 display values derived by post-event calculations based on daily medians from 7 days centred on the day of interest. Figs. 2, 3, and 4 display values smoothed over 7 days, while the remaining Fig. 5 displays averages over 4 months.

892

893
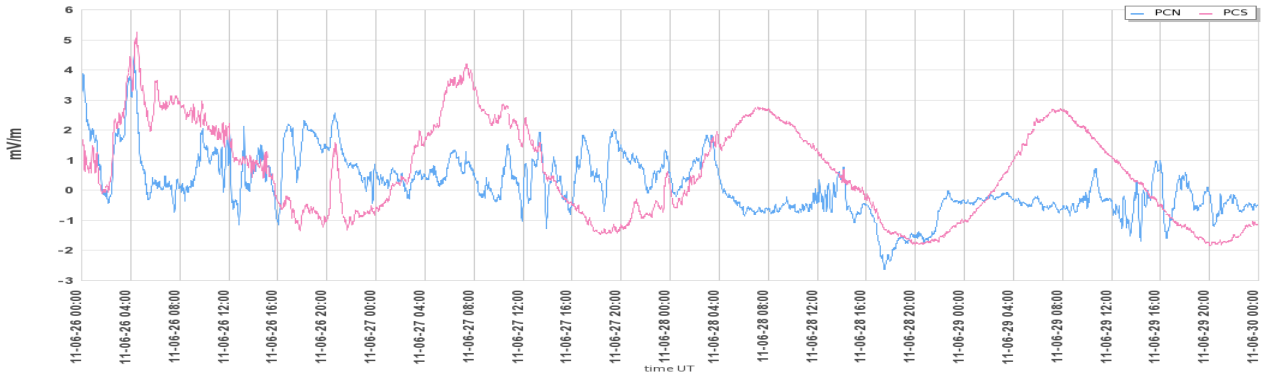
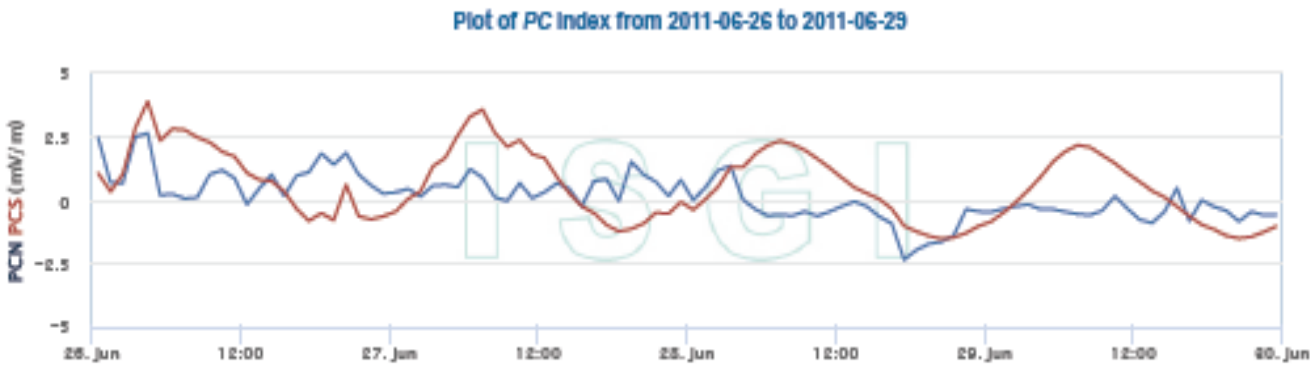894   **Appendix A2 (for the review process only).**

895   Appendix A2 presents further examples of erroneous archival PCS data like the one displayed in
896   Fig. 12 of the manuscript. Examples with quiet conditions have been selected for display as the
897   unjustified PCS excursions are then easy to detect. PCN/PCS examples have been downloaded from
898   the graphical output of the otherwise excellent AARI web site http://pcindex.org and from the ISGI
899   portal http://isgi.unistra.fr on 27 January 2020. The corresponding PCN and PCS index series
900   derived by using the DMI post-event calculation methods are displayed in the bottom diagrams.

901

902   **A2-1. PCN/PCS 26-30 June 2011**
903   **a. AARI archival web:**

904
905

906   **b. ISGI archival web:**

907
908
909

910   **c. DMI post-event calculations:**

911
912
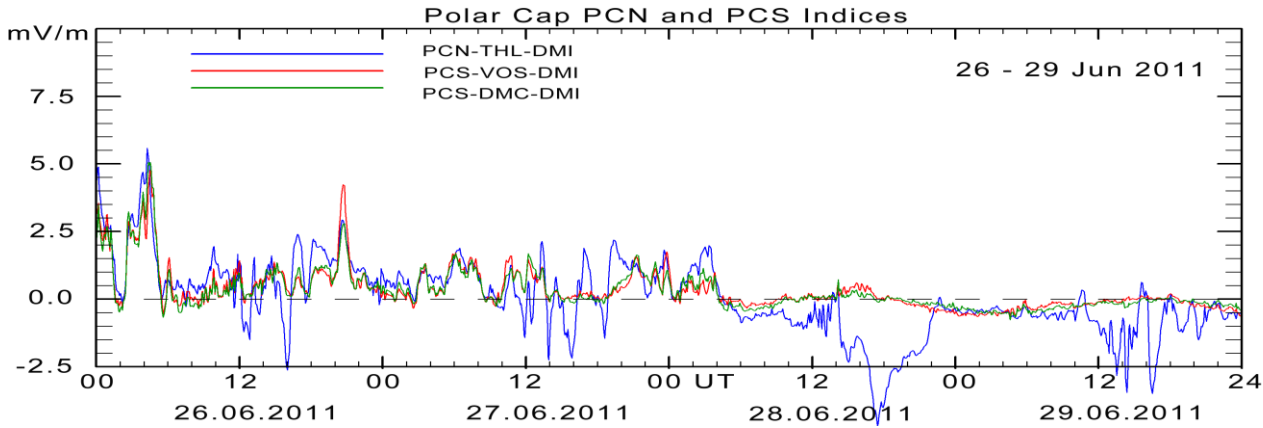
913 **A2-2. PCN/PCS 23-26 September 2011**
914 **a. AARI archival web:**

915
916

917 **b. ISGI archival web:**

918
919

920 **c. DMI post-event calculations:**

921
922
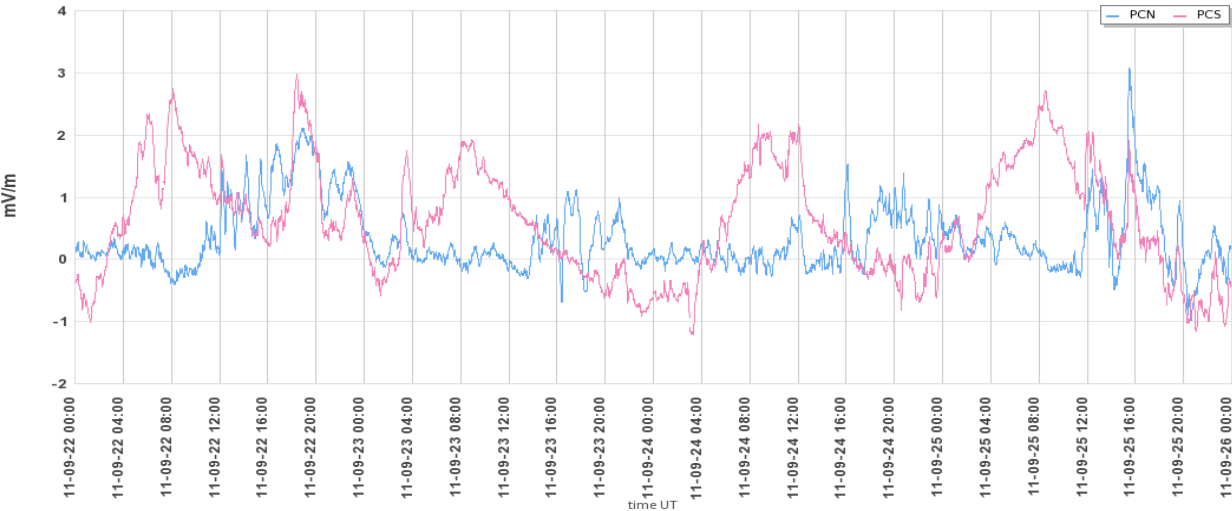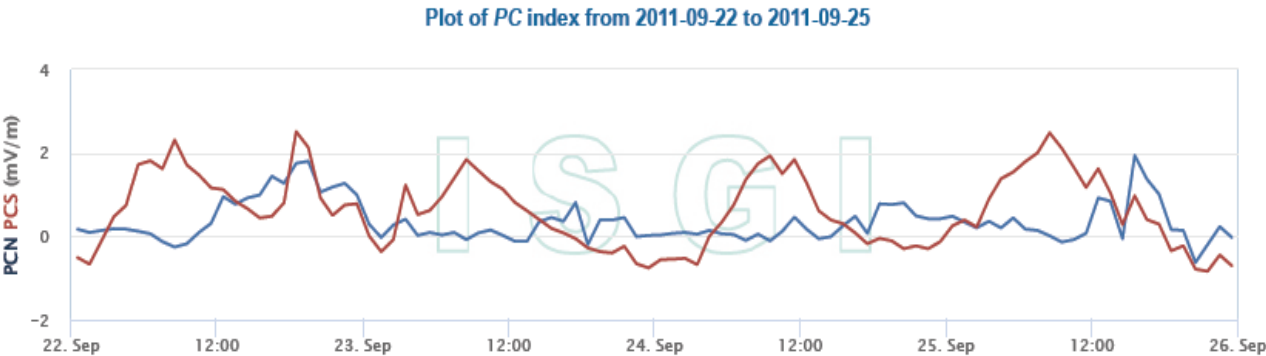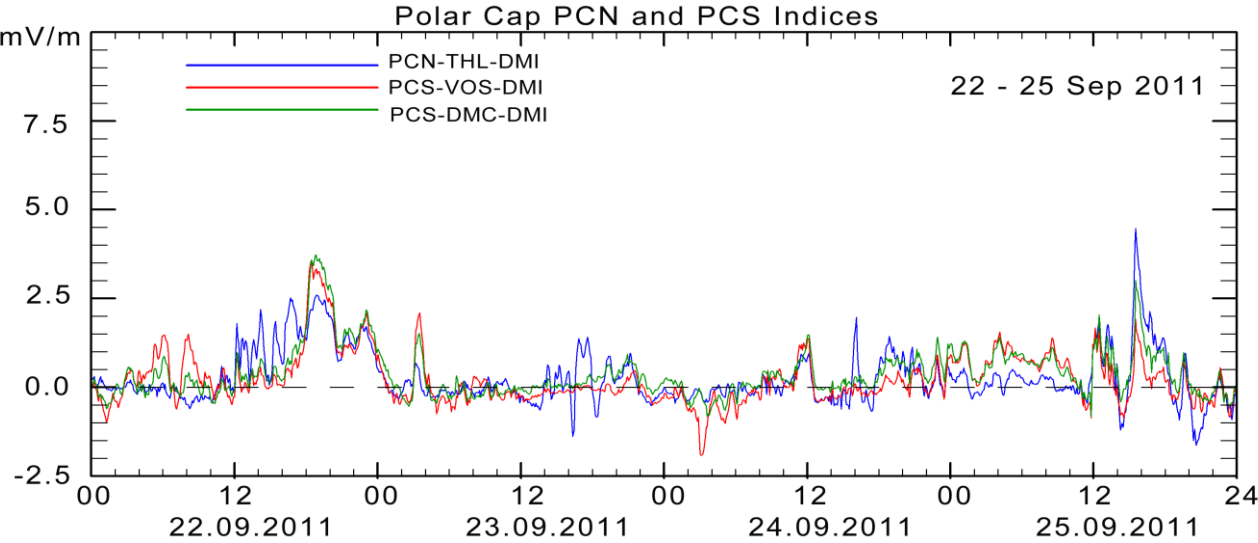
923 **A2-3. PCN/PCS 17-21 November 2011**
924 **a. AARI archival web:**
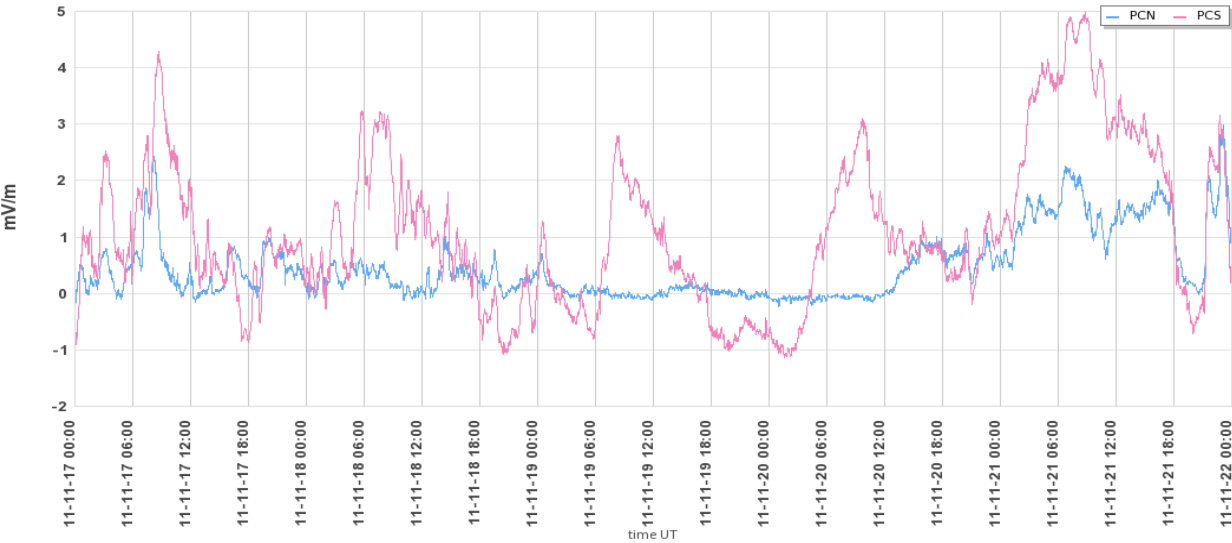
925
926
927

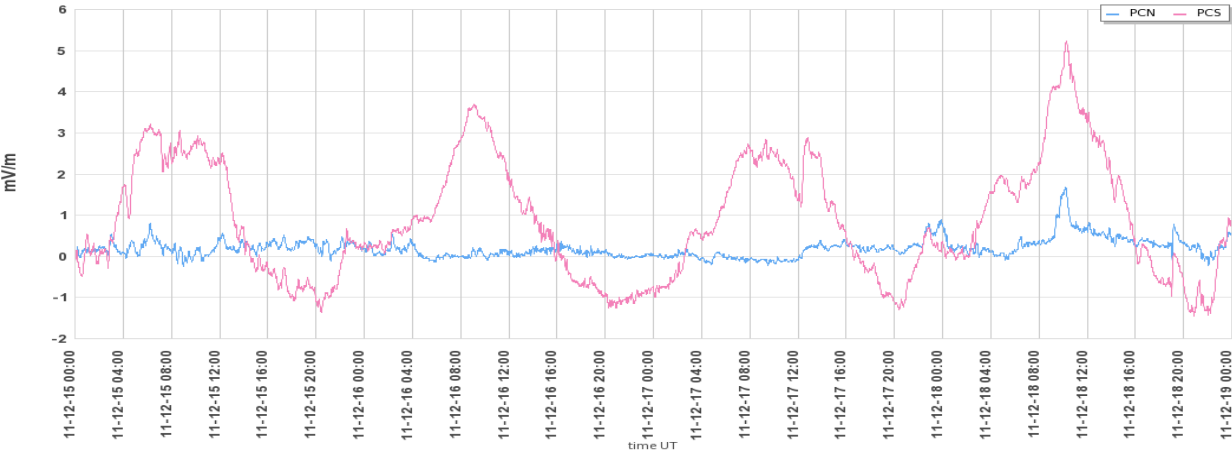928 **b. ISGI archival web:**

929
930

931 **c. DMI post-event calculations:**

932
933
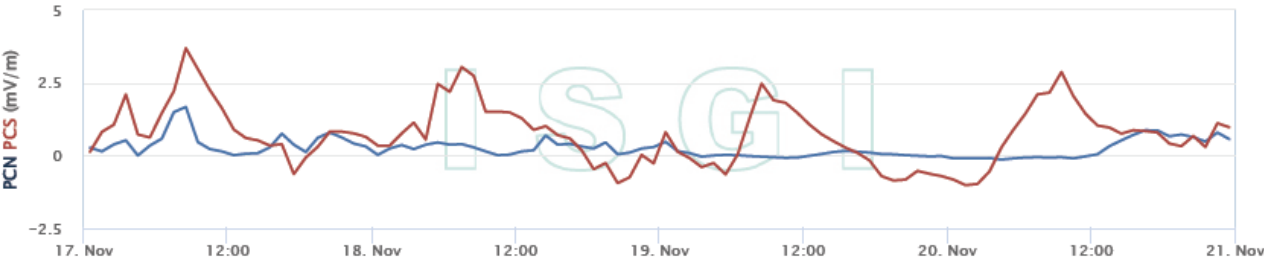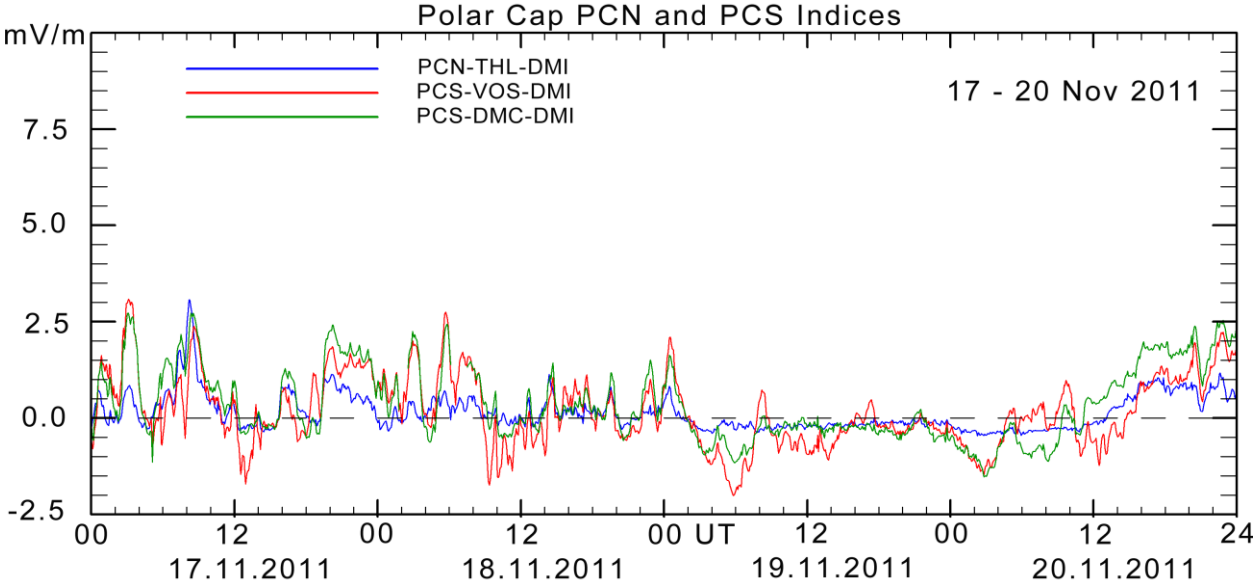
934   **A2-4. PCN/PCS 15-18 December 2011 (also in Fig. 12 of manuscript)**

935   **a. AARI archival web:**

936
937

938   **b. ISGI archival web**:

939
940
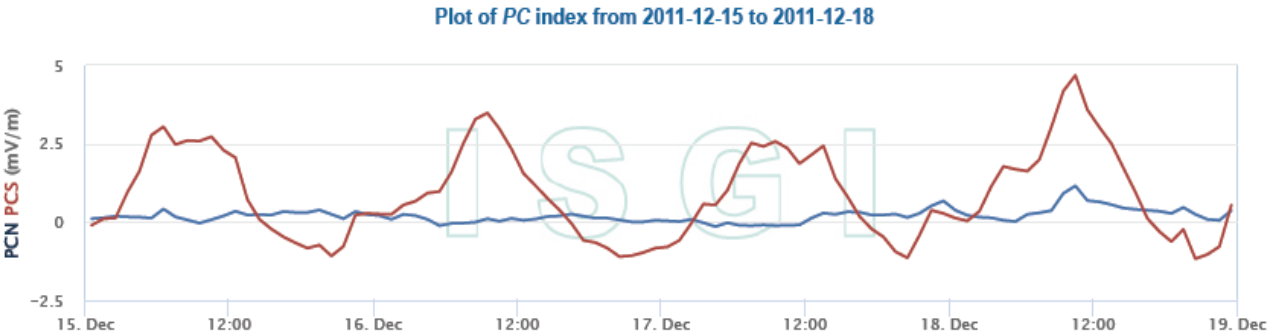
941   **c. DMI post-event calculations**

942
943
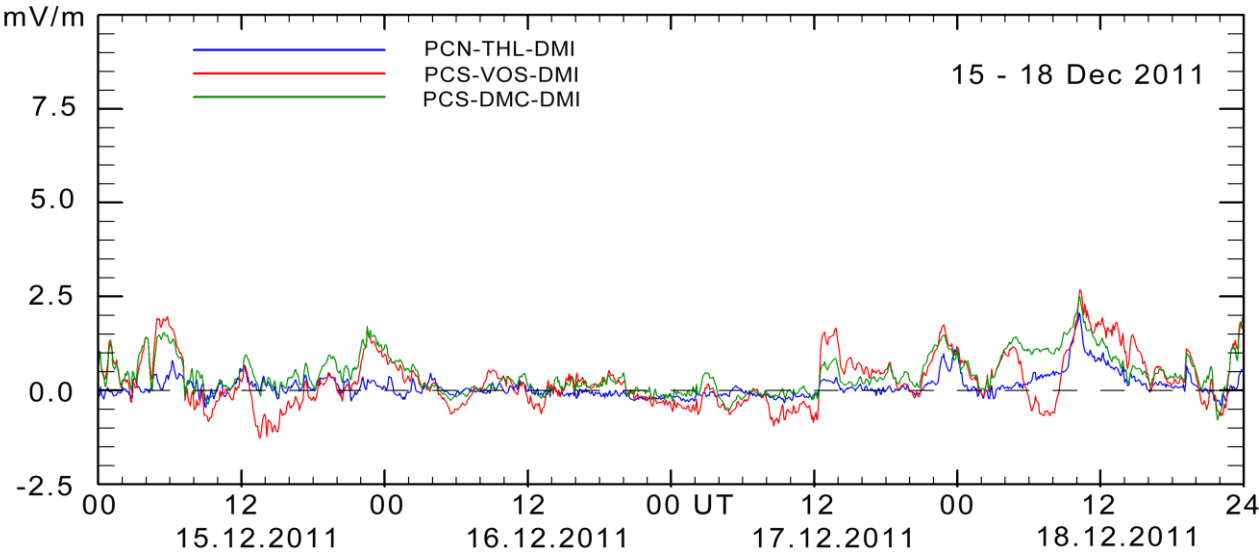
A2-5. Summary.

The PCS problem was detected in 2017 and notices of the problem was sent to the IAGA-approved PC index suppliers, Arctic and Antarctic Research Institute (AARI) in St. Petersburg, Russia, and DTU Space in Lyngby, Denmark during 2018. Notices have also been sent to the International Service for Geomagnetic Indices (ISGI), and to IAGA representatives. The problem, furthermore, was specified in the publication by Stauning (2018b).

The basic problem in the post-event (archival) PCS series displayed in Figs. A2-1a,b to A2-4,a,b of appendix A2 is the occurrences of unjustified daily excursions ranging between appr. -1.5 and +4 mV/m. The real PCS variations appear to be superimposed on the erroneous daily excursions, Since magnetic storm conditions are considered to apply at PC index levels exceeding 1.5 mV/m (Troshichev et al., 2017), such excursions of up to 4 mV/m would indicate (or hide) strong magnetic storms. The examples presented above are just a few among many corresponding cases in the series of provisional PCS values. They have been selected because of their appearance during quiet conditions, where the unfounded excursions are easy to detect. The magnetic data for these examples have been obtained from INTERMAGNET data service (http://intermagnet.org), where they are labeled as "final values". It is difficult to assess the data handling problem at AARI since there is no available description of the PCS derivation procedure.

Strictly speaking, the provisional PC index data should not be used in scientific works. However, the index suppliers (AARI and ISGI) have not cautioned against the use of their PCS index series and these indices have been used in several publications (e.g. Troshichev and Sormakov, 2015, 2017; Troshichev et al., 2014) without making notices of the potential problem.

With the DMI post-event data processing such excursions are absent as it appears from the PC index plots at the bottom of each of the above pages. These plots present PCN values derived from geomagnetic data from Qaanaaq (THL) in blue line. Furthermore, the plots indicate that the PCS indices derived from Dome C data (green line) are close to the values derived from Vostok data (red line). Thus, using both sources for deriving comparable PCS indices might enhance the reliability of using the indices for Space Weather applications as well as in general geophysical studies (Stauning, 2018b).